LBL--14489

DE82 020542

LBL-14489

Zero-field Spin Relaxation of the Positive Muon in Copper

Carl William Clawson

Nuclear Science Division
Lawrence Berkeley Laboratory
University of California
Berkeley, CA 94720

Ph.D. Thesis

July 1982

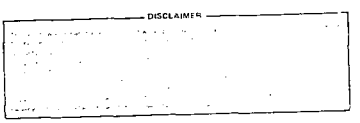

This work was supported by the Director, Office of Energy Research, Division of Nuclear Physics of the Office of High Energy and Nuclear Physics of the U.S. Department of Energy under Contract DE-AC03-76SF00098.

Zero-field Spin Relaxation of the Positive Muon in Copper

by

Carl William Clawson

ABSTRACT

The spin relaxation of the μ^+ in high purity single crystal and polycrystalline copper has been measured at temperatures between 0.5 K and 5.2 K by the zero-field μ^+SR technique. In both types of sample the experiments show a temperature independent dipolar width $\Delta_z = 0.389 \pm 0.003\ \mu s^{-1}$ and a hopping rate decreasing from $\sim 0.5\ \mu s^{-1}$ at 0.5 K to $\sim 0.05\ \mu s^{-1}$ above 5 K. This is the first direct proof of a dynamic effect in the low temperature μ^+ spin relaxation in copper.

The relationship between the zero-field and transverse-field dipolar widths is discussed, and the measured zero-field width is found to be ~10% larger than expected based on the known transverse-field widths.

A new μ^+SR spectrometer has been constructed and used in this work. The spectrometer and the associated beam lines and data acquisition facilities are discussed.

TABLE OF CONTENTS

CHAPTER I

INTRODUCTION

A. The μSR Technique

The work to be presented in this thesis is an experimental study using the techniques of positive muon spin rotation (μ^+SR). Polarized positive muons (μ^+) are implanted one at a time into the experimental sample, and for an ensemble of ~10^7 decay events $\mu^+ \rightarrow e^+ + \nu_e + \bar{\nu}_\mu$ the time interval between the arrival of the muon and the detection of the positron (e^+) is measured. For each of several e^+ detectors a histogram of the time values is collected. Since the angular distribution of the positrons is asymmetric with respect to the μ^+ spin direction, the histogram for a detector can be analyzed to yield the spin polarization of the μ^+ ensemble, projected on the detector direction, as a function of time. Several reviews of the subject[1-3] describe the experimental techniques, and a more detailed discussion will be given in chapter II.

If the μ^+ is stopped in a magnetic field H_o perpendicular to its polarization, its spin precesses at the Larmor frequency $\omega_o = \gamma_\mu H_o$ in the local field H_o. If the local field consists of the applied field plus a random field that varies from one muon to the next, e.g. nuclear dipolar fields at different sites in a crystal, the ensemble polarization will decay at a rate proportional to the magnitude of the random field. The signal resulting from this is essentially a

time domain free induction decay spectrum--its Fourier transform would give the line shape that would be obtained in a radio-frequency absorption experiment. This constitutes the conventional transverse-field μ^+SR technique, which has been the backbone of μ^+SR research for about 10 years.

Of great importance in this work is the zero-field μ^+SR technique,[4] pioneered by the University of Tokyo group, wherein no applied magnetic field is present; the μ^+ feels only the local magnetic fields created by the sample. Here the name "muon spin rotation" is somewhat inaccurate; we should call it muon spin relaxation instead. The spectrum observed in this case contains no oscillations (at least in non-magnetic metals), but the relaxation of the d.c. polarization can be observed. The relaxation envelope, however, is not the same as would be seen in transverse field. As we shall see in chapter III, it is especially sensitive to dynamic relaxation, i.e., to changes in the local field at the muon during its lifetime.

The behavior of the μ^+ in materials and the regime in which we can make measurements with μ^+SR are determined by several of its fundamental properties, which are listed below.

(see next page)

lifetime	$\tau_\mu = 2.20 \times 10^{-6}$ s
magnetic moment	$\mu_\mu = \frac{1}{207}\mu_e = 9 \times 10^{-23}$ esu cm
gyromagnetic ratio	$\gamma_\mu = 8.51 \times 10^{4}$ s^{-1} Oe^{-1}
	$= 2\pi \times 13.55$ kHz/Oe
charge	$+e = 4.8 \times 10^{-10}$ esu
mass	$m_\mu = 105.7$ MeV/c $= 207\, m_e = \frac{1}{9} m_p$
spin	$1/2$

The measurements are limited in time by the finite muon lifetime; magnetic fields that we may be concerned with must be on the order of a gauss or larger.

B. History of the Problem

In 1972, Gurevich et al.[5] reported the first measurements of the μ^+ spin relaxation in copper. This experiment was done in a magnetic field perpendicular to the initial muon polarization, and the resulting precession signal exhibited a temperature dependent relaxation rate. This was attributed to dipolar magnetic fields from the neighboring Cu nuclei, with temperature dependence caused by motional narrowing due to diffusion of the μ^+. From data taken between 77 K and room temperature (Fig. 1) they extracted the μ^+ hopping frequency ν and fit it with an Arrhenius law

$$\nu(T) = \nu_0 e^{-Q/T} \qquad (I.1)$$

with an activation energy $Q = 540$ K (45 meV) and a preexponential factor $\nu_0 \cong 3 \times 10^7$ s^{-1}. This implies that the μ^+ is essentially stationary below about 80 K, i.e., the hopping time at that tempera-

ture is much longer than the muon lifetime.

The relaxation rate was defined independently of the shape of the relaxation as the inverse of the time required for the polarization to decay to 1/e of its initial value. However, this parameter was used to compare a Gaussian relaxation function to the 77 K data with good agreement, indicating that the μ^+ is stationary, or nearly so, at this temperature. The relaxation rate was found to be $\sim 0.22\ \mu s^{-1}$ for T=77 K.

Further work[6] extended the temperature range down to 30 K and showed that the value of the preexponential constant was far smaller than it should be if the diffusion were due to classical over-barrier hopping, and that the activation energy was less than the barrier height known for hydrogen diffusion. A simple model of tunneling through a rectangular barrier using plausible values for the width and height was used to explain the results. In this picture, the activation energy Q represents the work needed to "prepare" the adjacent site by expanding it to fit the μ^+, but the overall barrier height is still important as it determines the tunneling rate. It was also noted that the temperature dependence deviated from the Arrhenius law at the high and low ends of the temperature interval studied.

Pursuing these studies, Camani, et al. investigated the orientation, magnetic field, and temperature dependences[7-10] of the transverse relaxation. When combined with the work of Hartmann[11] concerning the quadrupole effect on the dipolar line width, the

results that emerged seemed like a relatively complete and consistent picture of the μ^+ diffusion in copper: the μ^+, trapped at an octahedral (O) interstitial site in the Cu lattice, diffuses via a thermally activated process giving a spin relaxation well described by the "Abragam formula"[12] (which is actually due to Kubo and Tomita[13]) using the Van Vleck[14] value for the dipolar width at high field and a correlation time governed by an Arrhenius law temperature dependence. At lower fields the dipolar width is changed from the high field value due to the precession of the Cu nuclear quadrupoles in the electric field gradient that exists around the μ^+. The high-field relaxation was explained by assigning the μ^+ to an octahedral interstitial site and allowing the nearest-neighbor separation to be increased by about 5% due to the expansion of the lattice around the μ^+.

To be fair, we should note that the first mention of the approximate orientation independence of the relaxation rate in low fields was published by Hartmann, et. al.[15]

Theoretical support for this model has come from the work of H. Teichler.[16-20] He has calculated the hopping rates of the hydrogen isotopes, including the μ^+, in Cu using the quantum mechanical diffusion theory of Flynn and Stoneham[21] and Kagan and Klinger.[22] His approach uses non-linear screening to describe the muon-electron interaction and a pseudopotential to represent the screened μ^+-lattice interaction. With the Born-Oppenheimer approximation, these yield potential energy curves (Fig. 2) which show a shallow local

minimum at the tetrahedral (T) site and an absolute minimum at the O site.

His conclusion is that the μ^+ diffuses due to weakly lattice activated tunneling between neighboring octahedral sites. This is in contrast to the case of the isotopes H, D, and T, for which the tetrahedral site can support metastable bound states, whereas the lighter mass of the μ^+ causes its zero-point energy to lie above the top of the well. The heavier isotopes diffuse via O→T→O phonon-assisted over-barrier hopping whereas the μ^+ tunnels directly between ground state levels at octahedral sites. Since the energy levels of the μ^+ are changed by the lattice distortion, the μ^+ can't tunnel until a lattice fluctuation causes a level coincidence between neighboring sites. The activation energy for the hopping of this strongly self-trapped "small polaron" state is then just the lattice deformation energy necessary to equalize the μ^+ ground state levels at adjacent sites. This explains the small value of Q found in Refs. 5 and 6.

This "tunneling-hopping" theory also explains the deviations from the Arrhenius law seen in the experiments as a result of the zero-point fluctuations of the lattice modes as compared to the thermally excited phonons.

By 1980, then, it appeared the the μ^+ in Cu was well understood. In particular, the μ^+ seemed completely "frozen" below about 80 K. At that time Hartmann et al.[23] announced their observation at CERN of a decrease in the μ^+ transverse-field depolarization rate below 4 K

(Fig. 12). They interpreted this result as being due to motional narrowing: the μ^+ mobility increases as T is reduced below about 4 K.

In light of the previous knowledge this is a somewhat startling result, and one must consider the alternatives. In particular one should be careful about inferring motion from changes in the transverse-field relaxation. The reason is that much transverse-field work does not discriminate well between static and dynamic relaxation. The difference between static and dynamic processes depends critically on the shape of the relaxation function, not just on the relaxation rate. A static process yields a transverse relaxation function closely resembling a Gaussian (Gaussian line shape); whereas a dynamic process, where the field seen by an individual muon is not constant throughout the muon's lifetime, gives an exponential relaxation (Lorentzian line shape).[12] This can be understood heuristically by comparing a spin that precesses linearly from its initial orientation with one performing a random walk.

The shape of the relaxation function was not well measured in the experiments of Ref. 23; they assumed a Gaussian shape and stated that the data showed no clear preference for one shape versus the other. Thus their result is a shape-independent measurement and could be due to the μ^+ finding a different site to occupy at lower temperatures, for instance because of the presence of a high concentration of a shallow trap. The difference in the resulting nuclear dipole sum could explain the reduced depolarization rate.

We should note that in later communications from the CERN group,[24,25] they do mention difficulties with a Gaussian fit at the lowest temperatures; however they still use the Gaussian and make no mention of attempts to use exponential or Abragam relaxation functions. In addition, Ref. 25 presents data which do indicate that the μ^+ site is probably octahedral at the lowest temperatures, although the orientation dependence is weakened, presumably smeared out because of the motion of the muon.

It therefore became desirable to conduct a zero-field experiment in order to help distinguish among these alternatives. In this work the results of such an experiment[26] are presented. We have shown that the zero-field relaxation clearly indicates that the decrease in the relaxation rate below 5 K is due to motion of the μ^+.

A principal result of the theory of zero-field relaxation is that the polarization approaches 1/3 as $t\rightarrow\infty$ if the local field is time-independent. In our experiments the μ^+ polarization in zero field recovers nearly completely to an asymptotic value of 1/3 for long times at 5.2 K; below 2 K the recovery is completely suppressed. As we shall see in chapter III, the asymptotic polarization of 1/3 is a consequence of only the isotropy and static character of the local field distribution, so this constitutes a direct and unambiguous proof of the dynamic nature of the low temperature relaxation. No assumptions about possible locations of the μ^+ or details about the distribution in magnitude of the local field are required.

CHAPTER II

EXPERIMENTAL TECHNIQUES

A. Spectrometer and Beam Lines

The experiments were conducted at the Tri-Universities Meson Facility (TRIUMF), operated by University of British Columbia, University of Victoria, Simon Fraser University, and University of Alberta at the U.B.C. campus in Vancouver, B.C., Canada. The cyclotron produces an external 500 MeV proton beam with an intensity of 30-100 μA, which strikes a pion production target, typically a few mm or cm in size, producing copious quantities of secondary charged particles, primarily pions, muons, and electrons. The secondary particles are collected, momentum-selected, and delivered in a beam to the experimenter by magnetic optics.

A.1. μ^+ Production and Transport

In a conventional μ^+ beam,[1] μ^+ are collected from the "in-flight" decay of π^+, which gives rise to μ^+ of typically 100 MeV/c momentum. These μ^+ have a range of order 10 g cm^{-2} in matter. The μ^+ are slowed in a degrader material (usually polyethylene) and pass through several plastic scintillation counters into the sample. A counter behind the sample is used to veto the event if the μ^+ emerges from the sample, determining if the μ^+ has stopped in the sample.

The range spread of the μ^+ after passing the degrader is still sufficient to require the use of thick ($\geq$ 1 g cm^{-2}) targets in order to stop an appreciable fraction of the incident muons. The μ^+ are focused to a spot ~ 3-5 cm in diameter, so the optimum target size is of order 3 x 3 x 3 cm^3.

This is a rather sizable piece of material. Many interesting materials in solid state physics are rare or expensive, or for other reasons difficult to obtain in such sizes. Outside of solid state physics proper, one may wish to stop μ^+ in gases, powders, or other low-density targets. This is made possible by the use of the "surface muon" beam (also known as the "Arizona" beam) which results from the decay of pions at rest in the laboratory.[27]

When the proton beam is incident on the production target, sizable numbers of pions are created which do not escape the target. Those that are near the surface of the production target can emit a muon which escapes the target.

Considering the elementary kinematics of the two-body decay of a spinless particle ($\pi^+ \rightarrow \mu^+ + \nu_\mu$), and noting that the neutrino is left-handed and massless, we have two important facts in the pion rest frame (laboratory frame):

(1) The μ^+ is 100% polarized opposite to its momentum, and

(2) the μ^+ is monochromatic, p_μ = 29.8 MeV/c (kinetic energy T_μ = 4.1 MeV/c).

The first point is advantageous; it guarantees us maximum asymmetry in the μ^+SR signal, but the second point is the most important property for our purposes. The range of the surface μ^+ is ~150 mg cm^{-2} with a range width of ~30 mg cm^{-2} (Fig. 3).

An additional advantage of the surface μ^+ is seen from consideration of beam optics. A conventional μ^+ beam is obtained by first selecting pions of a given momentum, allowing them to decay in flight, and tuning the later section of the beam line slightly above or below the mean pion momentum to select muons which decayed in the forward or backward directions, respectively, relative to the pion momentum. The decaying pions form an extended source of muons so the beam spot is usually large. Surface muons, however, all emanate from the pion production target, an image of which is focused on the experimental target. There is also an advantage in that the solid angle for accepting pions is now 2π, rather than a few tens of msr. With good optics, beam spots as small as ~1 cm in diameter FWHM with very sharp edges have been obtained, and a flux of over 10^6 μ^+/s can be delivered into a 5 cm^2 spot.[28] Thus experiments on samples as small as 1 cm × 1 cm × 0.5 mm are possible, representing a factor of $\gtrsim 10^2$ decrease in the total mass of sample needed.

The short range of the surface μ^+ provides another advantage. A μ^+ beam is likely to be contaminated with significant numbers of positrons, in some cases as many as 100 for every muon. At the higher momenta of conventional muons, both muons and positrons are minimum-ionizing and hence have similar energy losses in scintilla-

tion counters. But the energy loss of a 29.8 MeV/c μ^+ is a factor of ~10 above the minimum-ionizing value, allowing pulse height discrimination between muons and positrons.

The short range of the surface μ^+ also creates one primary disadvantage: the μ^+ beam must be transported from the pion production target to the experimental target, and the amount of intervening matter must be small. For example, it is possible to fully stop a surface muon beam in about 1 m of air. It is necessary at the very least to pass the μ^+ through a scintillation counter, and the enhanced energy loss mentioned in the last paragraph aids in the solution of this by allowing the use of thinner scintillators.

The surface μ^+ also suffer multiple Coulomb scattering in passing through windows and counters. In the present apparatus the primary source of this is a 0.003" mylar window 6" upstream from the target, which will cause a mean scattering of 0.15" at the sample. To estimate the effect of multiple scattering, we make a worst-case assumption that the unscattered beam uniformly fills a 0.7" beam spot. Upon convolving this with a Gaussian scattering distribution, it is found that ~1% of the beam is stopped outside the 1" target diameter. This is negligible for our purposes.

A.2. Detectors

To take full advantage of the properties of surface muons, we have built a μ^+SR spectrometer (Fig. 4), dubbed "Eagle", designed specifically to utilize them. The chief constraint to be met is to

transport the μ^+ to the target through as little matter as possible. This is achieved by having the entire array of counters as well as the sample situated in the same vacuum chamber.

A 0.003" mylar window immediately upstream from the beam counter is necessary to isolate the experimental vacuum chamber from the beam line and cyclotron vacuum. The μ^+ pass this window and a 0.012" scintillator ("D" counter) before entering the target. These two items yield a total thickness of 42 mg cm^{-2}. Additional windows, etc., in the target assembly must be thin enough to keep the total thickness upstream of the sample below 100 mg cm^{-2}.

Four positron telescopes consisting of 1/4" thick plastic scintillators (L1-L2, R1-R2, F1-F2, B1-B2) are arranged parallel and perpendicular to the beam direction. The F and B counters are provided with holes in order to pass the μ^+ beam and, in the case of F, to pass any beam e^+ which penetrate the target. The solid angle subtended by the four counters is about 2/3 of 4π, and the net efficiency for detecting decay positrons, including dead time, is about 20%.

The D counter has a covering of 0.0003" aluminized mylar on each side, and the e^+ counters are covered with 0.001" aluminized mylar. UVT Lucite light guides from the scintillators exit the bottom of the vacuum chamber through O-ring seals and enter photomultiplier (RCA 8575) assemblies. The light guides outside the vacuum chamber are covered with aluminum foil and black vinyl wrapping. The entire scintillator, light guide, and phototube assembly is mounted on the

bottom cover plate of the vacuum chamber, which is in turn supported by Acme thread screws and sprockets in order to facilitate entry into the vacuum chamber.

Between the positron counter telescope elements are placed blocks of graphite to act as positron moderators. This helps to increase the positron asymmetry by cutting off the low end of the positron energy spectrum[1] and, more importantly, helps prevent scattered 29.8 MeV beam positrons from firing an "e" coincidence, which can be a troublesome source of noise.

Immediately upstream of the beam counter is a 1" thick brass collimator with tapered holes from 0.2" to 0.7" in diameter selectable from outside the chamber. This serves to define the beam entering the sample. This thickness and position of this collimator are such that positrons from muons stopped in it have very low probability for firing any of the "e" coincidences. Three additional one inch thick brass collimators of diameters 1.0", 1.125", and 1.25" are placed further upstream to protect the B2 counter from beam particles and to reduce the number of μ^+ which stop in the final collimator.

The target assemblies are inserted through the top of the vacuum chamber.

A.3. Magnetic Fields

A pair of water-cooled Helmholtz coils of mean diameter 22" surrounding the vacuum chamber is used to provide a transverse (vertical) magnetic field at the sample. Although in principle these mag-

nets can reach 6.5 kOe the low magnetic rigidity of 29.8 MeV/c muons prevents the use of fields above about 1 kOe. The field is controlled by regulating the current through the coils. The current is measured using a resistive shunt and converted to a field with the factor 4.63 Oe/A, which was measured by a Hall probe and by the μ^+SR precession frequency in aluminum. With this configuration we can measure both transverse components of the polarization with the e^+ telescope pairs (L-R) and (F-B).

A small pair of air-cooled coils is used to create longitudinal fields of up to 10 Oe. With no vertical field applied this allows measurement of the longitudinal polarization in fields from 0-10 Oe with the F and B telescopes. These coils are used primarily for compensating stray longitudinal fields.

The scintillator and vacuum chamber assembly are constructed of non-magnetic materials to preserve the field homogeneity and linearity at the sample. For the zero-field runs the stray magnetic field of ~1.5 Oe at the sample position was measured with Hall probes and reduced to < 0.2 Oe with appropriate currents in the two sets of coils. This reduces the background precession of the μ^+ to $\leq 1^{\circ}/\mu s$.

A.4. D.C. Separator

The spectrometer has been used successfully in 3 different beam areas of TRIUMF, the M13, M9-F2, and M9-W3 areas, but the experiments described here were performed primarily on the M9-W3 beam line due to its exceptionally clean μ^+ beam. This is achieved by the use of a

Wien filter velocity selector, which uses crossed transverse d.c. electric and magnetic fields to pass only particles of a given velocity. The 29.8 MeV/c beam positrons, which are extremely troublesome in a longitudinal measurement, are not selected against by purely magnetic optics, which pass all particles of a given charge and momentum. A selection by velocity following momentum selection allows only a single species of particle to reach the experimental area, and we obtain a beam with undetectably small positron contamination.

Because the zero-field μ^+SR technique depends critically on the behavior of the polarization at long times where the counting rate is quite low, the cleanliness of the beam is of great importance.

B. Data Acquisition

The conventional time-differential μ^+SR measurement[1] is used. The signals from the phototubes are discriminated and fed into the system of NIM logic shown in Fig. 5, which performs the e^+ coincidences and rejection of "bad" events. A 1 GHz time digitizer (TRIUMF model B080), or "clock", receives a start pulse at the time t_μ that the μ^+ passes the beam counter and a stop at the time t_e that an e^+ passes any of the telescopes L, R, F, B. A routing bit is sent to a coincidence buffer (Model C212, EG&G Ortec, Oak Ridge, Tenn. 37830) according to which e^+ telescope fired, and for each telescope a histogram of "good" events vs. $(t_e - t_\mu)$ is accumulated in the memory of a PDP-11/40 minicomputer and periodically updated on a disk file. The data are written into the PDP-11 memory by a CAMAC system driven by

an MBD-11 microcomputer interface, and on-line graphic display programs show the data as they are being accumulated. The data acquisition system has been described by Garner.[29] No event by event logging of data is done; the raw data consist of these histograms. An overall time resolution of approximately 2 ns is achieved.

To obtain a histogram which reflects the time distribution accurately, certain "bad" events must be suppressed. In order that a given positron can be associated with the muon from which it was emitted, we require that only one muon be present in the sample at one time. A pileup gate (Model GP 100/N, EG&G Ortec), known as the "data gate", is used to allow a clock start only when a μ^+ arrives at least a time T after the last previous μ^+, where T is chosen to be several μ^+ lifetimes. The pileup gate is also used to reject events where a second μ^+ arrives within time T of a μ^+ which started the clock. Events are also rejected if more than one positron is seen during the period T after the arrival of the μ^+. Timing diagrams for typical "good" and "bad" events are shown in Fig. 6.

The two-muon rejection effects a limitation on the ultimate rate at which one accepts μ^+. If the arrival times of the μ^+ are governed by Poisson statistics, then the "good" event rate R_g is related to the incident muon rate R and the gate length T by[29]

$$R_g = R \cdot \exp(-2TR) \quad . \tag{II.1}$$

R_g exhibits a maximum at $R=(2T)^{-1}$, so with a typical gate width of 10 μs the maximum usable incident muon rate is about 50 kHz, readily achieved at TRIUMF. At this rate we get typically 8,000-10,000 e^+/s,

depending somewhat on the target geometry and placement.

In using Poisson statistics, we have implicitly assumed that the cyclotron beam has no time structure. At TRIUMF under normal operating conditions the time structure occurs with a period of 43 ns, which is sufficiently smaller than the μ^+ lifetime that the Poisson assumption is valid. If the beam had a duty factor corresponding to a time structure of period much greater than a muon lifetime, then the effective rate would be decreased by that factor.

In practice, T is usually selected to be at least 8 μs, at which time only $2\frac{1}{2}$ % of the muons will remain. In principle, T could be made much shorter if one could make corrections for the incomplete rejection of "bad" events, or if one wants only to compare different samples. In practice, this can be dangerous, as the resulting distortions to the spectra are dependent on the instantaneous (up to ~1 MHz) μ^+ arrival rate, which may fluctuate with time.

All events which appear "good" at the time of the clock stop pulse activate "e Gate", which causes a CAMAC service routine to be requested at the end of the data gate. If subsequent second muons or electrons arrive, a reject bit will be set so the event will be rejected by the software. A dead-time gate is activated on a "good e" and inhibits sensitive portions of the logic until cleared at the end of the CAMAC service routine. It is very important, however, that the pileup gate run continuously in order to keep track of μ^+ arriving during the "computer busy" condition.

The rejection of second muons is the primary feature of the data acquisition system, especially since on the M9-W3 beam line there are no beam electrons so one in principle rarely gets a second e^+ without a corresponding second muon if T is long enough. But if the beam counter is not 100% efficient for μ^+, then some muons are able to "leak" in and cause distortions in the spectra. The requirement that D be highly efficient for μ^+ is somewhat contradictory to the requirement that its discriminator be set high enough to reject beam electrons. If a beam positron can fire D to give a start pulse, then a subsequent beam positron can scatter off the sample to give a "stop". Due to the time structure of the beam, this will appear as a 23 MHz noise signal in the spectrum.

An additional type of beam noise occurs when a beam positron fires an "e" coincidence after a muon caused a start. This will cause an exponential background to the data which actually appears flat if the beam electron rate is low. The carbon moderator suppresses these to a large extent, and in general it is better to leave the D discriminator set a bit low. It is much more harmful to get a few second muons than a few second electrons.

The problems with beam electrons are completely eliminated by the use of the electron-free M9-W3 beam, and the D discriminator can be set with a low enough threshold so as to be essentially 100% efficient.

The rejection of "bad" events is tested for by examining least squares fits to the observed spectra in transverse field of standard

targets, usually high purity aluminum. In the case of the "e-start, e-stop" events, examination of the Fourier transform for 23 MHz noise is used. On-line curve fitting and fast Fourier transform programs are available on the data acquisition computer so that these tests may be done as necessary during an experiment. On M9-W3, essentially perfect (chi-squared between 0.9 and 1.1) fits to high-statistics (3×10^6 events/histogram) data with backgrounds of $\leq 1\%$ are obtained and no 23 MHz is visible, indicating very adequate "bad" event rejection.

C. Cryogenics

C.1. 2 K to 300 K

Low-temperature experiments are conducted with a ^{4}He gas-flow cryostat (Model 10DT Super-VariTemp, Janis Research Co., Stoneham, Ma. 02180) with an optical tail extending down into the beam. Samples are inserted through the top with a removable positioner. The outer tail, which serves as a vacuum shield, is removed to eliminate its window from the total thickness the μ^+ must traverse. The cryostat insulating vacuum is contiguous to that surrounding the counters.

The μ^+ pass a 0.0003" aluminized mylar window in the 77 K radiation shield and a 0.005" mylar pressure window separating the sample space from the vacuum. The targets are mounted as close to this window as possible, because ^{4}He gas at 4.2 K has sufficient density (0.017 g cm^{-3}) to cause appreciable loss of μ^+ range over only a few cm. Accumulation of liquid ^{4}He up to the window level must be

avoided entirely, as 1 mm of it can completely stop the beam.

The temperature is controlled by a heater on the vaporizer assembly and by adjusting with a needle valve the flow of ^{4}He into the vaporizer. Adequate temperature stability (± 0.05 K at 5 K) for many experiments is obtained by running the heater at constant current and taking care that the pressure in the ^{4}He reservoir, which drives the liquid ^{4}He flow, remains constant. For more precise temperature stability, feedback from a thermometer on the sample can be used.

To obtain temperatures below 4.2 K, a mechanical rotary pump was used to reduce the pressure in the sample area. Care must be taken so that liquid ^{4}He is not drawn up around the sample when doing this. Temperatures down to about 2 K can be achieved in this fashion.

C.2. Below 2 K

For temperatures below 2 K, a ^{3}He single-shot evaporation refrigerator (Fig. 7) was fabricated. It consists of a copper cell containing several cm^3 of ^{3}He surrounded by an insulating vacuum space and upon which up to four samples are mounted with GE 7031 varnish. By pumping on the ^{3}He with a closed-cycle mechanical pumping station temperatures down to 0.5 K can be reached. The cell holds enough ^{3}He to maintain 0.5 K for > 6 h.

The ^{3}He refrigerator assembly was made as an insert for the Janis ^{4}He cryostat and is easily rotated to present the different samples to the beam. The vacuum/exchange-gas space around the reser-

voir is maintained by a surrounding can, provided with four 0.005" aluminized mylar windows for the beam. The Janis cryostat is used to reach 2 K with ~100-200 μ ^{3}He exchange gas present, ^{3}He is condensed in the cell, and the exchange gas is pumped out. The system is then ready for the ^{3}He cell to be pumped.

A carbon composition resistor was mounted on the bottom of the exchange gas can to sense liquid ^{4}He build-up in the tail of the Janis cryostat. Sample temperatures were measured with a calibrated Ge resistor (Model GR-200A-100, Lakeshore Cryotronics, Westerville, Ohio 43081) glued with GE varnish to the ^{3}He cell. Temperature was adjusted with metering valves on the ^{3}He pump inlet.

With this refrigerator in place, the total mass in the μ^+ beam upstream from the sample is approximately 90 mg cm^{-2}, including the two 0.001" Kapton windows in the d.c. separator on M9-W3.

D. Data Analysis

The observed spectrum for the i'th telescope is[1]

$$N_i(t)=N_{oi}\cdot\left[e^{-t/\tau}[1+A_i\vec{P}_\mu(t)\cdot\hat{n}_i]+B_i\right]$$

where N_{oi} is an overall normalization, A_i is the instrumental asymmetry of the telescope (the asymmetry that is seen for 100% μ^+ polarization), $\vec{P}_\mu$ is the μ^+ ensemble polarization, $\hat{n}_i$ are the telescope directions, B is a constant background term, and τ = 2.197 μs is the μ^+ lifetime. The data are analyzed in the simplest case by independent least-squares fits to individual telescopes, allowing N_o, A, B, and any parameters in $\vec{P}_\mu(t)$ to float. This is valuable in order to

check for agreement among the telescopes, but more properly one should calculate a chi-squared as a sum on all the telescopes since the parameters entering into $\vec{p}_\mu$ are common to all telescopes. In practice, with 4 telescopes this becomes difficult as too many parameters result for the available computer programs to vary simultaneously, so we instead fit two opposing telescopes at a time when using this method. τ may also be floated for an empirical check of bad event rejection since two-muon events lead to an apparent μ^+ lifetime shorter than 2.2 μs. The MINUIT[30] minimization program was used to obtain least-squares fits to the data and to generate statistical errors.

In a transverse-field experiment the spectra become

$$N_i(t)=N_{oi}\{e^{-t/\tau}[1+A_i G_x(t)\cos(\omega t-\phi_i)]+B_i\}$$

where ϕ_i is the angle of the i'th telescope with respect to the beam direction and we have introduced the transverse relaxation function $G_x(t)$. Fig. 8a shows a typical example of a transverse-field μ^+SR spectrum, and Fig. 8b shows the asymmetry $AG_x(t)\cos(\omega t-\phi)$ obtained from the raw data by dividing by $N_o e^{-t/\tau}$ after subtracting $N_o B$. The envelope of the oscillations in Fig. 8b is the interesting information provided by the experiment.

In the longitudinal geometry, only two telescopes (B,F) give any information, and the spectra are

$$N_F=N_{oF}\{e^{-t/\tau}[1-A_F G_z(t)]+B_F\}$$

$$N_B = N_{oB}\{e^{-t/\tau}[1+A_B G_z(t)]+B_B\} .$$

In this case, the damping of the polarization is described by the longitudinal relaxation function $G_z(t)$, which is in general not the same as $G_x(t)$.

Because of the very short range of the surface μ^+, few μ^+ stop outside of the sample. For this reason, it is unnecessary to perform background subtractions if the sample is large enough to fill the beam spot. Subtractions of this sort are performed in the experiments of Ref. 23 and contribute to their difficulty in determining the shape of $G_x(t)$. Experiments on high purity silicon at 15 K with this spectrometer on M9-W3 have shown diamagnetic asymmetry less than 0.005, which sets an upper limit of ~2% for the number of μ^+ stopping in the diamagnetic material around the sample.

CHAPTER III

THE DIPOLAR RELAXATION OF THE μ^+

We now turn to a more detailed examination of μ^+ spin relaxation phenomena than that presented in the Introduction. As mentioned there, relaxation of the μ^+ polarization can be caused by local magnetic fields from the randomly oriented nuclear dipoles in the material. It is the purpose of this chapter to discuss the nuclear dipolar spin relaxation of the μ^+ with an emphasis on the relationship of the transverse-field and zero-field methods. Much of the material in this chapter has been discussed in publications of the University of Tokyo group,[4,31,32] who have performed semiclassical calculations of moments and relaxation functions. Here we use a quantum mechanical approach where possible, since this proves to be necessary in order to understand the effect of the nuclear electric quadrupole interaction.

Since frequency units are the most natural in this work, we will use units such that $\hbar=1$ throughout this chapter.

The general quantum mechanical problem is to find the eigenvalues and eigenstates of the Hamiltonian for the coupled spin system of the μ^+ and N identical nuclei in the applied field $\vec{H}_0$:

$$\mathcal{H} = \mathcal{H}_{Z\mu} + \mathcal{H}_{ZI} + \mathcal{H}_{\mu I} + \mathcal{H}_{II}$$

where $\mathcal{H}_{Z\mu}$ and $\mathcal{H}_{ZI}$ are the muon and nuclear Zeeman energies, and $\mathcal{H}_{\mu I}$ and $\mathcal{H}_{II}$ are the muon-nucleus and nucleus-nucleus interactions. We

can break $\mathcal{H}$ into an unperturbed Zeeman Hamiltonian[33]

$$\mathcal{H}_o = -(\gamma_\mu s_z + \gamma_I \sum_i I_z^i)H_o$$

and a perturbing dipolar Hamiltonian

$$\mathcal{H}_d = \gamma_\mu \gamma_I \sum_i \frac{1}{r_i^3}\left[\vec{s}\cdot\vec{I}^{\,i} - 3(\vec{s}\cdot\hat{r}_i)(\vec{I}^{\,i}\cdot\hat{r}_i)\right]$$

$$+ \gamma_I^2 \sum_{j<k} \frac{1}{r_{jk}^3}\left[\vec{I}^{\,j}\cdot\vec{I}^{\,k} - 3(\vec{I}^{\,j}\cdot\hat{r}_{jk})(\vec{I}^{\,k}\cdot\hat{r}_{jk})\right]. \qquad \text{(III.1)}$$

Here $\vec{s}$, $\vec{I}^{\,j}$ are the spin operators of the muon and the j'th nucleus, γ_μ, γ_I are their respective gyromagnetic ratios, $\vec{r}_i$ is the position of the i'th nucleus with respect to the μ^+, and $\vec{r}_{jk}$ is the relative position of the j'th and k'th nuclei.

Note the relative magnitudes of the two terms of $\mathcal{H}_d$. The term $\mathcal{H}_{II}$ is much smaller than $\mathcal{H}_{\mu I}$ since $\gamma_\mu \gg \gamma_I$ (for copper, $\gamma_\mu/\gamma_I = 11.7$). The effect of this term is to cause nuclear spin flips at a rate $\sim 0.01\ \mu s^{-1}$, which is negligible for our purposes, and we drop $\mathcal{H}_{II}$ in all subsequent work. In the particular case of copper, it has been shown[34] experimentally that the nuclear spin relaxation rate is small ($\sim 0.01\ \mu s^{-1}$ in ^{63}Cu) and temperature independent.

A. The Static Relaxation

We assume in this section that the μ^+ is fixed in position, so that all $\vec{r}_i$ in Eq. III.1 are constant in time. The density matrix formalism is used to find the ensemble average of the expectation value of the μ^+ spin operator $\vec{s}$. This is given in the Heisenberg representation by

$$\langle \vec{s}(t) \rangle = \mathrm{tr}\, \rho \vec{s}(t)$$

$$= \mathrm{tr}\, \rho e^{i\mathcal{H}t} \vec{s}\, e^{-i\mathcal{H}t} ,$$

where ρ is the (time independent) density operator of the μ^+-nuclei system. We take $\vec{s}$ written with no argument to be the Pauli spin-$\frac{1}{2}$ operator $\vec{s} = \frac{1}{2}\vec{\sigma}$.

Since we shall always have $kT >> \gamma_I H_o$, we assume the nuclei are unpolarized. With the density matrix for a μ^+ with initial polarization $\vec{p}$, $\rho_\mu = \frac{1}{2} + \vec{p}\cdot\vec{s}$, this yields for the total density matrix for the system,

$$\rho = \frac{1}{(2I+1)^N} \left(\tfrac{1}{2} + \vec{p}\cdot\vec{s} \right) .$$

The desired quantity becomes

$$\langle \vec{s}(t) \rangle = \frac{1}{(2I+1)^N} \mathrm{tr}\, [(\vec{p}\cdot\vec{s})\vec{s}(t)] , \qquad \text{(III.2)}$$

where we have dropped the term $\mathrm{tr}\, \vec{s}(t) = 0$.

A.1. Transverse-field

We have $H_o \| \hat{z}$, $\vec{p}(0) = \hat{x}$ and we seek $\langle s_+(t) \rangle$. Eq. III.2 reduces in this case to[35]

$$\langle s_+(t) \rangle = \frac{1}{2(2I+1)^N} \mathrm{tr}\, [s_- s_+(t)] .$$

$$\propto \exp(-i\omega_o t)\, \mathrm{tr}\, [s_- \tilde{s}_+(t)]$$

where $\tilde{s}_+(t)$ is the interaction representation operator

$$\tilde{s}_+(t) = \exp(-i\mathcal{H}_o t) s_+(t) \exp(i\mathcal{H}_o t) ,$$

and $\omega_o = \gamma_\mu H_o$ is the center frequency of the line. From this we see

that the envelope of the oscillations is given by the relaxation function

$$G_x(t) = \frac{\mathrm{tr}\,[s_- \mathcal{S}_+(t)]}{\mathrm{tr}\,[s_- s_+]} .$$

The remaining piece of $\mathcal{H}_d$, that is, $\mathcal{H}_{\mu I}$, can now be written in terms of the spherical angular momentum components, which will help us to see the effects of the various terms. This is a standard procedure in NMR[36,37] and we will not give all the algebra. The result is

$$\mathcal{H}_d = \gamma_\mu \gamma_I \sum_i \frac{1}{r_i^3}[(1-3\cos^2\theta_i)s_z I_z^i + (\text{terms in } s_\pm I_\mp,\ s_z I_\pm,\ s_\pm I_z,\ s_\pm I_\pm)] ,$$

where θ_i is the polar angle of $\vec{r}_i$.

From this it is easy to see that only the term in $s_z I_z$ (known as the secular term), which commutes with $\mathcal{H}_o$, can cause a first order energy shift of any muon Zeeman level. The effect of the non-secular terms is to cause slight admixtures of states of differing energy;

$$|m_\mu, m_I\rangle \rightarrow |m_\mu, m_I\rangle + \lambda \cdot \left[|m_\mu \pm 1, m_I\rangle + |m_\mu, m_I \pm 1\rangle + |m_\mu \pm 1, m_I \mp 1\rangle + |m_\mu \pm 1, m_I \pm 1\rangle \right] ,$$

where λ is symbolic of a small quantity which decreases rapidly with the unperturbed energy differences. The result of this is to allow weak transitions at frequencies far from the line of interest, the closest being at $\omega_o \pm \gamma_I H_o$. Only if these satellite lines approach

within approximately a line width (σ) of the main line can they appear as a broadening; otherwise they appear as separate lines. For $\omega_I = \gamma_I H_o >> \sigma$ these terms do not contribute to the width of the main line at ω_o.

This language is that of NMR, where one actually observes in the frequency domain. In the μ^+SR experiment one observes in the time domain, but one measures the relaxation by curve fitting as if only a single frequency were present. In fact, the satellite resonances are far too weak to be observed by μ^+SR. Thus the same reasoning applies in our case, and henceforth we proceed using the "truncated" dipolar Hamiltonian:

$$\mathcal{H}_d' = \gamma_\mu \gamma_I \sum_i \frac{1}{r_i^3}(1-3\cos^2\theta_i) s_z I_z^i \ .$$

Since $\mathcal{H}_d'$ is just proportional to s_z, it is now easy to obtain an exact solution for $G_x(t)$. If we define $b_i = r_i^{-3}(1-3\cos^2\theta_i)$, the result is

$$G_x(t) = \prod_{i=1}^{N} \frac{1}{2I+1} \sum_{m_i=-I}^{I} \exp\left[i\gamma_\mu \gamma_I b_i m_i t\right]. \qquad \text{(III.3)}$$

By expanding the logarithm of G_x in powers of $\beta_i = \frac{1}{2}\gamma_\mu \gamma_I b_i t$, we obtain

$$G_x(t) \cong \exp[-\tfrac{1}{2}\sigma_{VV}^2 t^2] \ , \qquad \text{(III.4)}$$

where

$$\sigma_{VV}^2 = M_2^t = \frac{1}{3}\gamma_\mu^2 \gamma_I^2 I(I+1) \sum_i \frac{1}{r_i^6}(3\cos^2\theta_i - 1)^2. \qquad \text{(III.5)}$$

is the Van Vleck[14] value for the second moment. Note that this is also the second moment of the exact form as can be verified by differentiating Eq. III.3.

It should be noted that it has become conventional in experimental transverse-field μ^+SR to define $G_x(t) = \exp(-\sigma^2 t^2)$. The parameters are related by $\sigma = \sigma_{VV}/\sqrt{2}$.

A.2. Zero-field

In this case we use the initial μ^+ spin direction as the z axis; we have $\vec{P}(0) = \hat{z}$ and we seek

$$G_z(t) = \frac{\text{tr}\,[s_z s_z(t)]}{\text{tr}\,[s_z^2]} .$$

In the zero-field case we can not justify dropping the non-secular terms because there is no strong applied field to cause rapid precession of the nuclei. As the field is reduced to zero, the satellite lines which these terms create will grow and approach the main line and broaden it. Unfortunately, no simple solution for the relaxation function is possible in this case since the different components of $\mathcal{H}_d$ do not commute with one another. We can, however, use the method of moments in order to evaluate the zero-field second moment M_2^{zf} using the full dipolar Hamiltonian $\mathcal{H}_d$. This is done in an appendix; the result is

$$M_2^{zf} = \frac{1}{3}\gamma_\mu^2\gamma_I^2 I(I+1) \sum_i \frac{1}{r_i^6}(5-3\cos^2\theta_i) . \qquad \text{(III.6)}$$

A classical calculation of $\gamma_\mu^2\langle H_x^2+H_y^2\rangle$ keeping all components of $\vec{\mu}_I$

gives this same result.[4]

Note that for a μ^+ site with cubic symmetry, the sum of $\cos^2\theta_i$ over any shell of neighbors gives just the spherical average, $\langle\cos^2\theta\rangle=1/3$. In this case the zero-field width, in contrast to the transverse-field width, is isotropic. This will be the case, for instance, for the octahedral site in an fcc lattice.

The zero-field relaxation function can also be calculated directly from the Gaussian assumption, although the line shape is not simply an image of the local field distribution as in the transverse-field case. For a μ^+ in a local field $\vec{H}=(H_x,H_y,H_z)$, the time dependence of the z component of the spin expectation value is

$$s_z(\vec{H},t) = \cos^2\theta + \sin^2\theta\cos(\gamma_\mu|\vec{H}|t) ,$$

where θ is the polar angle of $\vec{H}$. If the local field is distributed according to $P(\vec{H})$, the observed relaxation function is[4]

$$G_z(t) = \int P(\vec{H})s_z(\vec{H},t)d^3\vec{H} .$$

(A similar approach may be used in an applied field.) If the local field distribution is isotropic, $P(\vec{H})d^3\vec{H} = H^2P(H)dHd\Omega$, we have

$$G_z(t) = \frac{1}{3} + \frac{2}{3}\int H^2P(H)\cos(\gamma_\mu Ht)dH . \qquad \text{(III.7)}$$

For P(H) a Gaussian with width $\gamma_\mu^2\langle H_i^2\rangle = \Delta^2$, we arrive at[4,38]

$$G_z(t) = \frac{1}{3} + \frac{2}{3}(1 - \Delta^2t^2)\exp(-\tfrac{1}{2}\Delta^2t^2). \qquad \text{(III.8)}$$

This function shows some interesting behavior: it initially decays as a Gaussian, $\exp(-\Delta^2t^2)$, and has a minimum at $t = \sqrt{3}\,\Delta^{-1}$ followed by a recovery of the polarization to an asymptotic value of

1/3 at time $t >> \Delta^{-1}$ (see the curve labeled $\nu = 0$ in Fig. 9a). The recovery to 1/3 is of special interest, as that particular feature is independent of the actual distribution in magnitude of the local field, as can be seen directly from Eq. III.7. Such behavior depends only on the local field being isotropic and static.

The behavior of the minimum at $t = \sqrt{3}\,\Delta^{-1}$ does depend on the Gaussian assumption. If one assumes a Lorentzian distribution of local fields, as in a dilute assembly of dipoles with random positions,[39] one finds a zero-field relaxation which exhibits only a very shallow minimum.[38,40]

The recovery of the polarization to 1/3 is very sensitive to changes in the local field during the muon lifetime, as this will cause the μ^+ spin to lose its memory of its initial direction. This will be made more quantitative in section B.

A.3. Comparison

To compare these formulae for M_2, we take a polycrystalline average to eliminate the angular dependence. With $\Delta_x^2 = \gamma_\mu^2\langle H_z^2\rangle$ we find for the transverse-field case,

$$\overline{M_2^t} = \Delta_x^2 = \frac{4}{15}\gamma_\mu^2\gamma_I^2 I(I+1)\sum_i \frac{1}{r_i^6}\,. \qquad \text{(III.9)}$$

For the zero-field case, with $\Delta_z^2 = \gamma_\mu^2\langle H_x^2\rangle$, we get

$$\overline{M_2^{zf}} = 2\Delta_z^2 = \frac{4}{3}\gamma_\mu^2\gamma_I^2 I(I+1)\sum_i \frac{1}{r_i^6}\,. \qquad \text{(III.10)}$$

We see that the zero-field second moment is a factor of 5 larger than the transverse-field value; the high field relaxation function initially decays only $(5)^{1/2}$ as rapidly as the zero-field function. Note that this is a combination of 2 effects. As the field is lowered to a value such that $\omega_I \sim \sigma$ the terms in $s_z I_\pm$, corresponding to the x and y components of $\vec{\mu}_I$, can now broaden the main line, which gives us the ratio of mean-square dipolar field components $\Delta_z^2/\Delta_x^2 = 5/2$. The nuclear dipoles are not precessing rapidly enough to average out their x and y components. As the field is lowered further so that $\omega_0 \sim \sigma$, we recover the terms containing $s_\pm$. The x and y components of the local field are now similar in magnitude to the z component and hence equally effective in relaxing the spin.

B. *Dynamic Effects*

The results presented in the preceding section are based on the assumption that random field components are either static or varying rapidly enough to be averaged out to zero. This section will be concerned with the case where hopping of the μ^+ causes fluctuations in the local field to occur during its lifetime.

Formally, motion of the μ^+ is obtained by adding an additional term to the Hamiltonian representing the μ^+ kinetic energy and its interaction with the lattice. The effect of this term can then be calculated by perturbation theory.[41] This leads to correlation functions which would be extremely difficult to evaluate. An approach more amenable to calculation is to let $\mathcal{H}_d' \rightarrow \mathcal{H}_d'(t)$, a random function of time, and make simple assumptions about its behavior.

In the transverse-field case, the relaxation function, equation III.3, can be thought of as the average $\langle \exp(-i\Omega t) \rangle$, where the average is taken over the various nuclear spin configurations and $\Omega = -\sum_i \gamma_\mu \gamma_I b_i m_i$ is the shift in the μ^+ Larmor frequency generated by the nuclear spin configuration $\{m_i\}$. If we allow $\mathcal{H}_d'$ to be time dependent, the time evolution operator becomes $\exp\left[-i\int_0^t \mathcal{H}_d'(t')dt'\right]$ and in terms of Ω we have

$$G_x(t) = \left\langle \exp\left[-i\int_0^t \Omega(t')dt'\right] \right\rangle .$$

Making the assumptions that Ω is a stationary Gaussian process with $\langle \Omega(t)\Omega(t-\tau) \rangle = \sigma^2 \exp[-\nu|\tau|]$, it is found that[12,13]

$$G_x(t) = \exp\left[-\sigma^2\nu^{-2}(e^{-\nu t} - 1 + \nu t)\right] . \qquad \text{(III.11)}$$

In the limit $\nu \to 0$ we recover the previous result

$$\lim_{\nu \to 0} G_x(t) = \exp\left[-\tfrac{1}{2}\sigma^2 t^2\right] ,$$

whereas in the limit of rapid fluctuations we obtain

$$\lim_{\nu \to \infty} G_x(t) = \exp\left[-\sigma^2\nu^{-1}t\right] .$$

This exhibits the phenomenon of motional narrowing. As the μ^+ begins diffusing more rapidly, the line becomes narrower and its shape changes from Gaussian to Lorentzian. In the limit of extremely rapid modulation, no relaxation occurs.

For hopping rates $\nu \ll \omega_I$, σ^2 will retain its static value of σ_{VV}^2. For more rapid hopping, the rapidly fluctuating fields can

facilitate recovery of the non-secular terms,[42] with a concomitant increase in σ^2. The application of this to μ^+ spin relaxation has been discussed by Hayano, et al.[4]

The application of the stochastic model to low- and zero-field relaxation was first considered by Kubo and Toyabe[38] in 1967. With the assumption of a Gaussian process for $\vec{H}(t)$, they derived $G_z(\nu,\Delta_z,t)$, recovering equation III.8 in the static limit. The sensitivity of the polarization for $t \geq \sqrt{3}\,\Delta_z^{-1}$ to the hopping rate ν was apparent from their treatment, but the problem was seen as academic due to the inability to measure the zero-field spin relaxation.

A further treatment was given recently by Hayano et al.[4,43] Instead of treating $\vec{H}(t)$ as a Gaussian process with an exponential correlation function, they assumed a strong collision model where the field after a hop is uncorrelated with that before the hop. This allows an exact solution for $G_z(t)$ to be obtained which is more suitable for numerical computation. The strong collision model gives essentially the same results as the Kubo-Toyabe model, although the latter gives a slightly stronger decay in the slow hopping ($\nu/\Delta < 1$) regime.

Curves of $G_z(t)$ and $G_x(t)$ with $\Delta_z^2 = 5/2\Delta_x^2$ are shown in Fig. 9. In order to see the relationship of the widths, the time axis in both cases is $\Delta_z t$. Because of the larger second moment, $G_z(t)$ decays more rapidly than $G_x(t)$. Also apparent is that a similar motional narrowing occurs in both for $\nu/\Delta \geq 1$. More important for many purposes, though, is the behavior of $G_z(t)$ for $t \geq \sqrt{3}\,\Delta_z^{-1}$. At

those long times, the recovery of the polarization to 1/3 is very sensitive to hopping with $\nu/\Delta<1$. Thus, in addition to motional narrowing, $G_z(t)$ exhibits "motional decay of the asymptotic polarization", or "motional broadening of the zero-frequency transition", which is far more sensitive to slow fluctuations of the local field.

The strong collision model has also been shown to be suitable for computation by a Monte Carlo treatment of the random field and the hopping process.[44-46] Kubo[40] has given a general treatment of the stochastic model from which these different models can be derived by making the appropriate assumptions about the process $\vec{H}(t)$.

C. The Quadrupole Interaction

In the preceding sections of this chapter, we have been concerned only with the Zeeman levels in the applied field $\vec{H}_o$ and the magnetic dipole interaction between the μ^+ and the nuclei. However, the naturally occurring isotopes of copper, ^{63}Cu and ^{65}Cu, both have spin 3/2 and electric quadrupole moments $Q\simeq-0.15 \times 10^{-24} cm^2$. An electric field gradient (EFG) caused by the lattice expansion about the μ^+ exists at the Cu nuclei, and the interaction of the EFG with their quadrupole moments has a strong effect on the dipolar relaxation.

The total Hamiltonian is now (assuming an axially symmetric quadrupole interaction)

$$\mathcal{H} = \mathcal{H}_{Z\mu} + \mathcal{H}_{ZI} + \mathcal{H}_Q + \mathcal{H}_d \ ,$$

where

$$\mathcal{H}_Q = \omega_Q \cdot \left[3I_Z^2 - I(I+1)\right] .$$

The Z axis is here taken along the direction of the EFG, which is different for each nucleus. Note that $\mathcal{H}_Q$ itself contains no μ^+ operators. Its effect on the μ^+ spin is to change the way in which the nuclear dipoles precess, therefore changing the truncation to be performed on $\mathcal{H}_d$.

Transverse-field

In transverse field, the importance of the quadrupole interaction can be parametrized by the ratio of magnetic to electric energies, ω_I/ω_Q (n.b.--for a spin-3/2 nucleus, the quadrupole splitting is actually $6\omega_Q$). This has been treated theoretically by Hartmann.[11] He has shown that if the magnetic field is sufficiently strong ($\omega_I/\omega_Q \gg 1$), the dipolar width σ_{VV}^2 (equation III.5) is seen, whereas in lower fields the relaxation is changed from this value. The reason is that the z axis (magnetic field direction) is no longer a unique quantization axis since nuclei now tend to precess about the directions of the vectors $\vec{r}_i$ connecting the μ^+ with each nucleus. In low fields, this precession can cause averaging of non-secular terms just as precession about $\vec{H}_o$ can.

This is treated formally in a similar fashion as the truncation of the dipole Hamiltonian in the high field case, section III.A, except the unperturbed Hamiltonian of the nuclei is now $\mathcal{H}_I^T = \mathcal{H}_{ZI} + \mathcal{H}_Q$. The energies and eigenstates of this are generally not simple, and one must numerically diagonalize $\mathcal{H}_I^T$ and truncate the nuclear spin operators appearing in $\mathcal{H}_d$ to remove the matrix elements

connecting different unperturbed energies. The μ^+ spin operators are treated the same as before since $\mathcal{H}_Q$ has no direct effect on the μ^+.

In the experiments of Camani, et al.[7,9,10] this theory was applied to measurements of the orientation and field dependence of the transverse-field relaxation rate. The data with theoretical curves are shown in Fig. 10. There are two principal effects that are noted.

(1) The high-field relaxation rates are given by the Van Vleck values with the nearest neighbor distances increased by 4.9%. From the high-field orientational dependence, it is concluded that the μ^+ resides in an octahedral interstitial site.

(2) The orientational dependence of σ is weakened by the quadrupole interaction at low fields. From the field dependence of σ, it is concluded that $\omega_Q = 1.1 \pm 0.1\ \mu s^{-1}$.

Zero-field

In zero field, Hartmann's calculations do not apply, but in this case the total unperturbed Hamiltonian is easily diagonalized, as it is simply $\mathcal{H}_Q$. In a basis where $\hat{r}_i$ is taken as the quantization axis, $\mathcal{H}_Q$ is diagonal and we can read off the eigenvalues $E_m = \omega_Q \cdot \left[3m^2 - I(I+1)\right]$. Then the nuclear angular momentum operators appearing in $\mathcal{H}_d$ can be truncated to remove the non-secular elements and calculate M_2. This would appear at first to amount to the removal of the nuclear spin components perpendicular to $\vec{r}_i$, but in the case of half-integral nuclei the degeneracy of $m=\pm 1/2$ allows static

components of $\vec{I}$ perpendicular to $\vec{r}_i$. This calculation is shown in an appendix, and the result is

$$M_2^Q = \frac{1}{3}\gamma_\mu^2\gamma_I^2 I(I+1)\sum_i r_i^{-6}\left[4\sin^2\theta_i + \frac{3(2I+1)}{8I(I+1)}(2-\sin^2\theta_i)\right] .$$

This form is correct for half-integral spins; for integral spins the second term in the brackets, which results from the degeneracy, is not present.

It should be noted that if the EFG is due to the presence of the μ^+, it will decrease with distance so that the truncation of the nuclear spins will no longer be valid for the higher terms in the sum. However, the relaxation is primarily due to the first shell of neighbors, so an error of <1% is made by extending the summation over all nuclei.

As mentioned above, expressions quadratic in cosθ are isotropic if the μ^+ has cubic surroundings, and we see the angular average width

$$M_2^Q(\text{cubic}) = \overline{M}_2^Q = \frac{8}{9}\gamma_\mu^2\gamma_I^2 I(I+1)\sum_i r_i^{-6}\left[1 + \frac{3(2I+1)}{16I(I+1)}\right] .$$

In the case of copper, I=3/2, this reduces to

$$\overline{M}_2^Q(I=3/2) = \frac{16}{15}\gamma_\mu^2\gamma_I^2 I(I+1)\sum_i r_i^{-6}$$

$$= \frac{4}{5}\overline{M}_2^{zf} . \qquad \text{(III.12)}$$

Since $M_2 \propto \Delta_z^2$, we see that the quadrupole effect is not very large, serving to reduce Δ_z by about 10%: $\Delta_z^Q/\Delta_z = \sqrt{4/5}$.

CHAPTER IV

EXPERIMENTAL RESULTS

A. Samples

Two copper samples have been used in this work. Most of the data have been taken with a sample referred to as the "LBL" copper. This is a slice of a high purity (5-9's, RRR~1800) oxygen annealed single crystal prepared at the National Bureau of Standards, Boulder.[47] The oxygen annealing was performed in order to precipitate residual iron impurities. The orientation is such that the initial μ^+ polarization (horizontal) is parallel to a <110> axis and the applied transverse magnetic field (vertical), if any, is parallel to a <111> axis.

Several runs were also taken on the copper sample used by the CERN group[23,25] in their transverse-field μ^+SR experiments. This is a very high purity (6-9's, RRR~6600) polycrystalline specimen purified by soluble anode electrolysis and high-vacuum melting.[48] The impurity content is estimated to be < 20 ppm interstitial (primarily C,N,O) and < 1 ppm substitutional.

B. Preliminary Studies

The first observations of the zero-field relaxation in copper were made in November 1979. This experiment was performed on the M13 beam line at TRIUMF using a provisional μ^+SR apparatus known as

"Beaver", which was mounted inside a large set of triaxial Helmholtz coils in order to compensate stray magnetic fields, primarily due to the beam line magnets and the main magnet of the cyclotron.

Data were taken at several temperatures from 40 K to 160 K on the LBL copper sample. The data were analyzed by simultaneously fitting the forward and backward spectra to the theoretical curves of Hayano, et al.[4] First, a run at 40 K was analyzed with $\nu = 0$ in order to obtain the values of Δ_z and the asymmetries, then these parameters were held fixed to these values for the rest of the runs. The value found for Δ_z was $0.375 \pm 0.010\ \mu s^{-1}$. The results for $\nu(T)$ are shown in Table I. Although these data were taken under conditions of severe beam positron background, the slow hopping of the μ^+ is clearly exhibited. An Arrhenius plot of these data is shown in Fig. 11, together with the Arrhenius curve for the best-fit parameters $\nu_0 = 210$ MHz and $Q = 900$ K. Also shown is an Arrhenius curve using the best known values[10] obtained from the transverse-field data, $\nu_0 = 44$ MHz and $Q = 620$ K. The parameters agree in an order-of-magnitude sense only.

Because of the large backgrounds and μ^+ lifetime distortions encountered in this run, it is believed that these data are only semi-quantitatively correct. Due to beam time constraints and the decommissioning of the M9 d.c. separator, it has not been possible to repeat these observations in order to obtain a more reliable measurement of the slow hopping near 100 K.

During August, 1980, the LBL copper was measured by transverse- and zero-field μ^+SR at 21.9 K with the Eagle spectrometer on M9-W3. The static recovery of polarization to 1/3 was clearly seen in these data. Only one set of spectra was taken, and it yielded $\Delta_z = 0.382 \pm 0.007\ \mu s^{-1}$ and $\nu = 0.05 \pm 0.02\ \mu s^{-1}$. The asymmetries were fixed to the values obtained by a transverse-field run for this analysis. In Fig. 15a the data from the B telescope are shown with the fit. The asymmetry is obtained from the raw data using the fitted values of N_o and B. The minimum in the polarization is clearly seen in these data, and the fit to the theory is very good.

C. Measurements Below 5 K

The transverse- and zero-field μ^+SR measurements were made on the CERN polycrystal and the LBL single crystal copper samples in two runs in 1981 using the ^{3}He refrigerator in the Eagle spectrometer on the M9-W3 beam channel. Zero-field runs and transverse-field runs at 80-100 Oe were alternated, and typically 10^7 events were taken in each run. Since the shape of the relaxation is of utmost importance in this work, a data gate length of 14-15 μs was used in order to have a minimum number of μ^+ which survive longer than the gate length. Data were taken in 8 ns bins out to 12 μs.

The transverse-field data were analyzed by fitting to a Gaussian relaxation function with all parameters variable, and for each of the telescopes F and B weighted averages of the asymmetries were taken over all runs done without disturbing the target. Because the transverse-field data contain oscillations, the asymmetry can be

determined much more accurately than in zero field, where the polarization has a smooth time dependence. As long as the target position and μ^+ stopping distribution remain constant, the asymmetry can be fixed by this method. There were two sets of runs taken, those numbered in the 100's during January, 1981, and those numbered in the 800's during June, 1981. For the January, 1981 data the asymmetries were $A_F = 0.252$ and $A_B = 0.196$, and for the June, 1981 data the values used were $A_F = 0.268$ and $A_B = 0.209$.

The transverse-field data are summarized in Table II. The agreement of the asymmetries is very good among members of each of the two sets of runs. Fig. 12 shows our transverse-field widths superimposed on those of Hartmann et al. The agreement is very good; that slightly higher values were obtained by us is probably due to the lower magnetic fields we used. Their field of 520 Oe is sufficient to cause a small reduction in the line width by quenching of the quadrupole interaction (Fig. 10). Also shown in Fig. 12 are the CERN data on aluminum, with one point measured in Al during our experiments shown. This shows that any "baseline" relaxation, due to applied field inhomogeneity, etc., is similar between the two experiments.

The zero-field data were analyzed by least-squares fitting to the strong-collision model for $G_z(\nu,\Delta_z,t)$. This was done in two stages. First, the curve fits were done with asymmetries taken from the transverse-field data, and both ν and Δ_z were allowed to vary. The results for Δ_z are shown in Table III, and Fig. 13 shows Δ_z

plotted as a function of T. From this we conclude that Δ_z is temperature-independent.

Next, a weighted average of the Δ_z values was taken, yielding $\Delta_z = 0.389 \pm 0.003\ \mu s^{-1}$. Δ_z was fixed to this value, and the fits were done again with only N_0, B, and \ varying. The resulting values for \ are shown in Table IV.

For these data, we have analyzed the F and B telescopes separately; the discrepancy seen in the \ values obtained is several times larger than the statistical error, and we take this as an indication of the level of systematic error in the measurement of \. A plot of \ vs. T is shown in Fig. 14. The F and B values are shown connected by a vertical line; the extent of this line above and below the data points shows the statistical error.

Note that two of the runs (runs 114 and 117) near 0.5 K show values for \ which appear to be systematically low. This may be due to some stopping of μ^+ in liquid helium accumulating in front of the beam since there were some difficulties in the operation of the ^{3}He cryostat during the January, 1981 run. We have rejected all runs where the accumulation of ^{4}He was apparent from the behavior of the cryostat, but a small effect on these runs can not be ruled out. Improvements to the cryostat, chiefly the use of ^{3}He as the exchange gas, were made between runs 129 and 132. This completely eliminated this problem, and we are confident that the "800" series of runs and the runs from the "100" series on the CERN sample represent the best data available.

Plots of the backward asymmetry for the three "800" series zero-field runs are shown in Fig. 15b,c,d. No significant difference exists between the data at 21.9 K and 5.15 K. At 2.35 K the loss of the recovery of polarization is complete, and at 0.63 K the onset of motional narrowing is easily visible.

The agreement between the polycrystal and the single crystal samples is good for both ν and Δ_z. The equality of Δ_z can be taken as evidence for the octahedral location of the μ^+ since, as mentioned above, the zero-field width is isotropic only for a site with cubic symmetry.

We have used the Gaussian relaxation function in fitting the transverse-field data shown in Table II in order to compare our data with those of Hartmann, et al. However, since the zero-field work clearly shows a temperature-independent width, a more proper analysis would be to hold the width constant and use Eq. III.11 to get the hopping rate ν directly. This has been done for the "800" series of runs, and the results are shown in Table V and Fig. 16, along with the hopping rates deduced from the zero-field method using a simultaneous forward-backward fit.

There is a clear discrepancy between the hopping rates given by the two methods. The reason for this is that the transverse-field data were taken at a field not sufficiently high to completely average the non-secular terms. Since these terms are then varying on a time comparable to the μ^+ relaxation rate, their effect is to create a fictitious addition to the hopping rate, which is, after all,

really a measure of the fluctuation times of the magnetic fields seen by the μ^+.

A quantitative calculation of this additional "pseudo-hopping" is quite difficult as it requires a solution to the equation of motion for the density matrix of the μ^+ spin and its nearest-neighbor nuclear spins. This treatment must also include the quadrupolar interaction, and enhancements of the relaxation may occur due to this as the quadrupolar level-splitting is near the μ^+ Zeeman splitting, leading to the possibility of quadrupole-induced muon spin-flips.

We have not attempted to perform these calculations, as the primary purposes for our taking transverse-field data were to provide the instrumental asymmetries for use in the zero-field analysis and to compare it with the CERN data. In any case, the hopping rate clearly increases as the temperature is lowered.

CHAPTER V

DISCUSSION AND SUMMARY

A. The Dipolar Width

Copper is an fcc metal with a cubic lattice constant of 3.61 Å and two abundant isotopes, ^{63}Cu (69.1%) and ^{65}Cu (30.9%). Both have nuclear spin 3/2 with similar gyromagnetic ratios and quadrupole moments, $\gamma(^{63}\text{Cu}) = 2\pi \times 1.1285$ kHz/Oe, $\gamma(^{65}\text{Cu}) = 2\pi \times 1.2090$ kHz/Oe, and $Q(^{63}\text{Cu}, ^{65}\text{Cu}) \cong -0.15 \times 10^{-24}$ cm^2. For calculations of the widths, the proper average of γ is the weighted mean square value, $\gamma_{\text{eff}} = 2\pi \times 1.154$ kHz/Oe, and we use this value in all work.

The theory presented in Chapter III shows that given these parameters, relaxation rates can be computed from first principles with only one adjustable parameter--the expansion of the nearest neighbors of the μ^+. Once this is known we can calculate the sums in Eqs. III.5 and III.6 to obtain the zero-field and high-field widths.

Transverse-field experiments[7-10] have provided us with this parameter. The best value available is 4.9%, given in Ref. 10 with no error quoted. An estimate of the error of this can be taken from Ref. 8, where the value $\sigma_{VV}/\sqrt{2} = 0.2589 \pm 0.0036\ \mu s^{-1}$ was quoted for the high-field relaxation rate for the <100> direction at 4500 Oe. This is in reasonable agreement with the value of $0.265\ \mu s^{-1}$ calculated from Eq. III.5 with a 4.9% nearest-neighbor expansion. When this is used in Eq. III.12 we obtain the expected value

$$\Delta_z(\text{theory}) = 0.350 \pm 0.005\ \mu s^{-1}\ ,$$

whereas the data presented in chapter IV showed that

$$\Delta_z(\text{experiment}) = 0.389 \pm 0.003\ \mu s^{-1}\ .$$

Note that the criterion for validity of truncating the nuclear spins is well satisfied, $\Delta_z/6\omega_Q = 0.06$.

The value of Δ_z and its error are taken from a weighted average of measurements at different temperatures. At any specific temperature, the statistical error of Δ_z is typically $\pm 0.010\ \mu s^{-1}$.

As mentioned in chapter III, the zero-field width is isotropic if the μ^+ site has cubic symmetry. The good agreement of single crystal and polycrystalline samples is evidence that the site is cubic at all temperatures studied, but a more sensitive test would be a measurement of the orientation dependence of the width in a single crystal.

It should also be pointed out here that an earlier measurement of copper in near-zero magnetic fields[49] yielded a similar value of $\Delta_z = 0.372 \pm 0.004\ \mu s^{-1}$, although the use of an incorrect fitting function and an incorrect calculation of the quadrupole effect on the width hindered the interpretation of this result.

We now consider several possible explanations for the disagreement between the transverse-field and zero-field dipolar widths.

(1) The EFG may not be in the radial direction and/or the quadrupole interaction may not be axially symmetric.

(2) The lattice distortion about the μ^+ may not have cubic symmetry.

(3) The μ^+ is not actually a point particle; rather, its wave function has a finite extension about the center of the O site.

(4) The EFG may be temperature dependent, leading to a breakdown of truncation at low temperatures. A $T^{3/2}$ temperature dependence has been suggested.[50]

No estimates have been made of the first two effects, but we should note that these are related by a point first proposed in Ref. 8. There it was suggested that the lattice distortion and resulting EFG were not due solely to the self-trapping distortions caused by the μ^+, but rather that the μ^+ are being trapped at energetically favorable sites in the strain field of a lattice imperfection. There would then exist a pre-formed EFG and lattice distortion, which would not be symmetric about the μ^+, and the simple theory we have used would be only approximate. The present experiment has shown consistent values of Δ_z for both single crystal and polycrystal specimens, which would indicate a limit on the deviation from cubic symmetry of the expansion.

Anomalies in the low field relaxation at low temperatures are seen in the transverse-field data of several workers in copper and other metals. These have been attributed to non-radial[10] or temperature-dependent[51] EFGs. No satisfactory understanding of this behavior exists, so it is likely that departure of the behavior of the EFG from the simple assumptions previously made can contribute to the deviation of Δ_z from the expected value.

If the μ^+ has a wave function $\psi(\vec{r})$, then its position must be averaged over to obtain the dipolar Hamiltonian,

$$\mathcal{H}_d \rightarrow \int \mathcal{H}_d(\vec{r}) |\psi(\vec{r})|^2 d^3\vec{r} .$$

No calculations exist which give the effect on the magnitude and isotropy of Δ_z due to the spread of the μ^+ ground state wave function. It has been shown[41] that if one assumes a spherical wave function, $|\psi(\vec{r})|^2 \propto \exp(-r^2/2a^2)$, the spread of the wave function will serve to decrease the value of $\mathcal{H}_d$ isotropically by a factor $\lambda(r/a)$ which approaches unity rapidly for $r > a$. Since all components of the nuclear dipole field at the μ^+ are decreased by λ, this cannot affect the transverse-field and zero-field widths differently.

This, as well as a lattice expansion about the μ^+, could thus be responsible for the decreased relaxation rates observed. However, the ground state wave function would not be spherical, so due to the different angular dependences of the zero-field and transverse-field widths, the reduction of the width could be different in the two cases, and could give an anisotropy in the zero-field width.

To estimate the size of this effect would require realistic wave functions for the μ^+, but we can note that λ increases rapidly from $\lambda = 0.5$ at $a = \frac{1}{2} r_{nn}$ to $\lambda = 0.85$ at $a = 1/3 r_{nn}$. In Cu these numbers are 0.9 Å and 0.6 Å respectively. If an anisotropy in the correction factor is to account for the difference in the transverse-field and zero-field widths, then we must have a spreading of the wave function of at least 0.6 Å. This could not be ruled out on the basis of the

potential energy curve given in Ref. 19 (Fig. 2).

It is likely that the extension of the ground state wave function at the μ^+ site is responsible for at least some of the reduction in σ_{VV} from the point-muon, unrelaxed-lattice value. This is also indicated theoretically, as the calculated value[19] of 0.03 for the nearest neighbor expansion is smaller than the 0.05 inferred from the experiments.

Note that the entire deviation of σ from its value for an unrelaxed lattice could be accounted for by a μ^+ wave function of width $a = 0.6$ Å even in the absence of a lattice expansion.[41]

B. Low Temperature Diffusion and Trapping

The second principal aspect of this work is the use of the zero-field μ^+SR method as a complement to the transverse-field method in determining the μ^+ mobility. We are able to clearly demonstrate that the reduction of the transverse-field line width seen by others is due to hopping of the μ^+ in a distribution of random local fields having a constant width. Quite apart from the magnitude of Δ_z, its temperature independence and orientation independence (inferred from the equivalence of single crystal and polycrystalline samples) provides evidence that the μ^+ moves among equivalent octahedral sites rather than migrating to different species of trapping sites at different temperatures.

Our experiments do not, however, give a clear indication of the mechanism of diffusion below 2 K. The theory of light-interstitial

diffusion has received a great deal of attention,[16-22,52-61] and a variety of opinion[62-66] exists as to the applications of the theory to understanding the experiments on μ^+ motion at low temperatures. We do not intend to present a comprehensive discussion of this subject here, but rather to touch on a few points of interest to the present case.

One of the central questions in the study of μ^+SR in metals is the possibility of observing the coherent motion of the μ^+, i.e. the incipient formation of a delocalized Bloch wave which would allow the μ^+ to propagate rapidly by tunneling through the lattice. This mechanism would show a decreasing hopping rate with increasing temperature because of the disruption of the narrow μ^+ energy band by phonons, but estimates of the temperature above which coherent tunneling should be negligible range from 10^{-17} K to 200 K.[63] Even if a completely delocalized wave cannot form due to lattice imperfections, local tunneling states with a spreading of the μ^+ wave function over a few adjacent sites may occur, and may actually be enhanced by the presence of defects.

However, even in a material that exhibits an intrinsic diffusion rate that increases with temperature, the presence of traps for the muons (for instance impurities or lattice imperfections) can result in an apparent decrease in the hopping rate as the temperature is increased.[67,68] A schematic transverse-field depolarization curve representing a crystal with a single species of trap is shown in Fig. 17. At very low temperatures, the intrinsic diffusion rate is small

and the depolarization is characteristic of the self-trapped state in the pure material. As the temperature is raised, the muons begin to diffuse faster, showing motional narrowing, and then begin to find traps, which causes again a strong localization and a corresponding high relaxation rate. The relaxation rate then remains roughly the same until a temperature is reached such that the muons can be thermally detrapped, and the relaxation curve once again approaches that for the pure material.

The relaxation curve of Fig. 17 is characterized by two temperatures, a trapping temperature T_t depending on the trap concentration and a detrapping temperature T_d proportional to the activation energy required to escape the traps. As shown in Fig. 17, the effect of increasing the trap concentration is to lower T_t thus decreasing the depth of the dip in the relaxation rate. Such behavior is in fact seen in N-doped Nb[69] where $T_t \sim 20$ K and $T_d \sim 80$ K.

If such a trapping model were invoked to explain the decrease of σ below 2 K in copper, the concentration of traps would need to be very high, since our zero-field data clearly show hopping rates $\lesssim 0.5\ \mu s^{-1}$, indicating that the traps must be found within only a few hops.

Petzinger[70,71] has shown that the zero-field method has a unique ability to distinguish trap-limited diffusion from intrinsic diffusion. In a simple model where the intrinsic diffusion is assumed rapid enough that depolarization occurs only at traps and where no detrapping occurs, he has calculated $G_z(r,\Delta_z,t)$ (Fig. 18), where r

is the rate at which the μ^+ distribution relaxes to the traps. This should apply to the zero-field spin relaxation in the region where σ shows an upward slope toward the defect-trapped state in Fig. 17.

Our data clearly contradict his result. The trap-limited $G_z(r,\Delta_z,t)$, like the Kubo-Toyabe function, shows a minimum in the polarization (for large enough r) but always recovers to an asymptotic value of 1/3. For $r\rightarrow\infty$ the static Kubo-Toyabe function, Eq. III.8, is recovered, but for slower trapping rates the minimum in $G_z(t)$ is lost and the polarization decays monotonically. Furthermore, the initial decay rate in this model shows large changes with r even at earlier times than at the minimum, whereas our data are clearly consistent with the Kubo-Toyabe theory where the initial decay rate is constant until the hopping becomes sufficiently rapid to cause a complete loss of the recovery of the polarization to 1/3. This indicates that the μ^+ experiences more than one non-zero, static value of the random magnetic field during the observation time.

A complete theory of relaxation/trapping would have to account for both relaxation at traps as well as relaxation while undergoing intrinsic diffusion between traps. However, since our data are well described by the Kubo-Toyabe model, we have no evidence for trap-limited diffusion in copper.

As noted by several authors,[25,63,71] the results obtained for $\sigma(T)$ in copper are remarkably insensitive to the purity of the material. The slope of $\sigma(T)$ near 150 K is similar in samples of very different purity, and our data show good agreement between two

samples of different purity in their behavior below 5 K. This indicates that if the trapping of the μ^+ is due to impurities, then they are present in high concentration in all copper samples.

One possible source of a high concentration of weak traps, small inhomogeneities in the lattice behavior due to the isotopic mixture of natural copper, has been ruled out by experiments[63] on isotopically pure (99.6%) ^{63}Cu. These measurements have shown no significant differences from natural copper. Although one cannot completely rule out trapping at the remaining concentration of ^{65}Cu or at chemical impurities, trapping by this mechanism seems to be unlikely in view of these observations.

Another potential source of traps is the presence of long range elastic strain fields[63,72] caused by interstitial impurities (C,N,O) in the crystal. A single impurity can facilitate trapping at many sites by this mechanism, so the concentration does not need to be high. (Impurities at the 100 ppm level can create strain fields throughout the lattice[73] which are sufficient to cause localization by the Anderson[74] mechanism.) We should also note that calculations[75] have shown that the strain fields may actually catalyze self-trapping at favored sites at the end of the muon thermalization process. If this were the case, the zero-field relaxation would not be expected to follow the theory of Petzinger, since the initial distribution of muons through the crystal would not be uniform. Instead, the muons would all be trapped essentially at t=0.

In summary, the high concentration of traps that would be required to give trap-limited diffusion at 5 K taken together with the sample purity independence of the relaxation behavior and the good agreement with the Kubo-Toyabe relaxation functions in zero field are all consistent with intrinsic diffusion in a pure copper host crystal. We cannot, however, rule out the possible role of long range strain fields as traps or trap-enhancers. Since there would be a distribution of trap energies and concentrations in that case, the simple model of Petzinger would be inadequate, and a Kubo-Toyabe behavior could be seen as the muons become trapped by deeper traps occurring in lower concentrations as the temperature is increased above 0.5 K.

C. Future Work

The study of the diffusion of the μ^+ through its spin relaxation is one of the oldest problems in modern μ^+SR research, and the development of the zero-field method has opened up new avenues of inquiry in this as well as other problems. In this work, we have by no means exhausted the possibilities for zero-field studies in copper. When the d.c. separator is recommissioned on the improved M20 channel, zero-field μ^+SR will again be feasible at TRIUMF, and several possibilities are suggested for further experiments.

First, a new measurement of the hopping rate in the range of 80 K to 150 K would be very valuable, especially in the slow hopping region inaccessible to transverse-field μ^+SR. This may yield important details about the validity of the quantum diffusion theory[16-22]

in this region, where so far the agreement with experiment[9,10] is very good. It may be possible to see further deviations from the Arrhenius behavior due to the temperature-dependent prefactor and activation energy given by the theory.

Second, the isotropy of Δ_z should be carefully studied in the region of 10 K to 80 K where minimum hopping exists. As we have shown, this will be sensitive to deviations from cubic symmetry of the lattice distortions and EFGs occurring about the μ^+ and/or spreading of the μ^+ wave function. This may yield important clues as to the nature of the trapped state of the μ^+, i.e. whether one sees self-trapping in the pure material or impurity-enhanced trapping in a pre-existing lattice deformation.

Third, the measurements should be extended to temperatures as low as possible. The transverse-field experiments show a plateau in σ below 0.5 K, but the sensitivity of the zero-field method to slow hopping may uncover structure which has gone heretofore unnoticed.

APPENDIX A

Zero-field Second Moments

The second moment can be calculated as

$$M_2 = - \frac{tr\{[\mathcal{H}_d', s_z]^2\}}{tr\,[s_z^2]} . \qquad (A.1)$$

We take the Z axis as the initial μ^+ spin direction. $\mathcal{H}_d'$ is the "truncated" dipolar Hamiltonian defined in the basis of the unperturbed eigenstates by $(\mathcal{H}_d')_{m,m'} = (\mathcal{H}_d)_{m,m'} \cdot \delta_{E,E'}$. The matrix elements of $\mathcal{H}_d$ which connect states of different unperturbed energy must be dropped. As argued in chapter III, these elements create separate lines rather than broadening the main line if their frequencies are far enough from the main line. We will drop the prime from $\mathcal{H}_d$ in what follows, it being understood that we will truncate it appropriately.

$\mathcal{H}_d$ is properly written as a sum over all nuclear dipoles, with the traces taken over the $(2I+1)^N(2s+1)$ states of the muon-nuclei system. But since the traces of terms containing products of operators for different nuclei vanish, we can calculate the moment for each nucleus individually and add the contributions when finished.

The calculation is most conveniently carried out in coordinates (x,y,z) where the z axis is along the radial direction for each nucleus. We then have

$$s_Z = s_z\cos\theta - s_x\sin\theta$$

and

$$H_d = \gamma_\mu\gamma_I r^{-3}[-2s_zI_z + \tfrac{1}{2}(s_+I_- + s_-I_+)]$$

Calling the operator in square brackets K, the numerator of equation A.1 is proportional to $\mathrm{tr}\{[K,(s_z\cos\theta - s_x\sin\theta)]^2\}$. We have $[K,s_z] = i[s_xI_y - s_yI_x]$ and $[K,s_x] = -i[2s_yI_z + s_zI_y]$, so

$$-[K,s_Z]^2 \rightarrow \cos^2\theta\cdot[s_xI_y - s_yI_x]^2 + \sin^2\theta\cdot[2s_yI_z + s_zI_y]^2$$

$$\rightarrow \cos^2\theta\cdot[s_x^2I_y^2 + s_y^2I_x^2] + \sin^2\theta\cdot[4s_y^2I_z^2 + s_z^2I_y^2] \ .$$

All traceless terms such as s_xs_y have been dropped. The traces of the μ^+ spin operators can now be eliminated. Remembering that the traces extend over the nuclear spin coordinates as well, we have

$$M_2 = \frac{\gamma_\mu^2\gamma_I^2 r^{-6}}{(2I+1)}\cdot\left\{\cos^2\theta\left[\mathrm{tr}_I I_y^2 + \mathrm{tr}_I I_x^2\right] + \sin^2\theta\left[4\mathrm{tr}_I I_z^2 + \mathrm{tr}_I I_y^2\right]\right\} . \qquad (A.2)$$

The notation tr_I indicates a trace over only the nuclear spin coordinates. To proceed further, we must specify the truncation to be performed on $\vec{I}$.

Pure dipolar case

If there are no quadrupole moments, the unperturbed Hamiltonian is absent and we use the full operator $\vec{I}$ in equation A.2. For any component of $\vec{I}$, $\mathrm{tr}_I I_j^2 = (1/3)I(I+1)(2I+1)$, and summing over all nuclei we have

$$M_2 = \frac{1}{3}\gamma_\mu^2\gamma_I^2 I(I+1)\sum_i r_i^{-6}[5 - 3\cos^2\theta_i] \ . \qquad (A.3)$$

Quadrupole case

If there is a quadrupole interaction of sufficient strength that its energy level spacings greatly exceed the line width, then we must remove all matrix elements of $\vec{I}$ between different energies. The quadrupole Hamiltonian is

$$\mathcal{H}_Q = \omega_Q \cdot [3I_z^2 - I(I+1)] ,$$

and we see that the eigenvalues are given by $E_m = \omega_Q \cdot [3m^2 - I(I+1)]$. Now $\vec{I}$ has non-vanishing matrix elements $\vec{I}_{m,m'}$ for $m=m'$ and $m=m'\pm 1$, and the only states for which these are degenerate are $m=\pm\frac{1}{2}$. The proper truncation is then:

(1) for integral spins, drop I_x and I_y completely, and

(2) for half-integral spins, drop all but the $m=\pm\frac{1}{2}$ elements of I_x and I_y.

The integral (I) case can now be disposed of immediately,

$$M_2^Q(I) = \frac{4}{3}\gamma_\mu^2\gamma_I^2 I(I+1)\sum_i r_i^{-6}\sin^2\theta_i \cdot \qquad (A.4)$$

For the half-integral (HI) case, we have the truncated operators

$$I'_{x,y} = \frac{2I+1}{4}\begin{bmatrix} 0 & \\ & \sigma_{x,y} \\ & & 0 \end{bmatrix} ,$$

where $\vec{\sigma}$ represents the Pauli matrices acting on the $m=\pm\frac{1}{2}$ states. From this we see that $\mathrm{tr}_I(I'_x)^2 = \mathrm{tr}_I(I'_y)^2 = \frac{1}{8}(2I+1)^2$, and we get[4]

$$M_2^Q(HI) = \frac{1}{3}\gamma_\mu^2\gamma_I^2 I(I+1)\sum_i r_i^{-6}\left[4\sin^2\theta_i + \frac{3(2I+1)}{8I(I+1)}(2-\sin^2\theta_i)\right] \cdot \qquad (A.5)$$

Acknowledgements

Experiments of this nature are by necessity the work of more than one person. For this reason, the "we" that appears in the text is usually intended as a plural pronoun and not as an editorial device. I would like to thank all the principal collaborators on the low temperature copper experiment--Ken Crowe, Steve Rosenblum, Jess Brewer, Chao-Yuan Huang, Jim Smith, and Stan Kohn. In particular, Chao-Yuan Huang, Jim Smith, Stan Kohn, and Steve Rosenblum performed most of the work of designing, fabricating, and testing the helium-3 refrigerator, and Jess Brewer and Steve Rosenblum performed much of the data analysis. These individuals have also contributed greatly to our other μ^+SR efforts at TRIUMF.

Special thanks must go to Ken Crowe, who as group leader has maintained a strong effort in μ^+SR even in the face of an uncertain funding situation.

I also extend my thanks to Dave Spencer, Dale Harshman, Don Fleming, Dave Garner, Rob Kiefl, Hugo Schilling, and Alex Schenck, who have, at one time or another, provided manpower and expertise when needed on the experimental runs. Rudi Abegg provided valuable assistance in the maintenance and operation of the helium-3 cryostat.

Tomo Uemura is thanked for helpful discussions and for stimulating my early interest in the problem, as well as for collaboration on the zero-field measurements at higher temperatures and for kindly

providing me with the results of his numerical computations of the zero-field relaxation function. I have also benefited from discussions of zero-field relaxation with Rolf Keitel, Bill Zajc, and Jim Bistirlich in addition to the principal collaborators mentioned above.

I am most grateful to Erik Karlsson and Alain Yaouanc for their generous permission to cut a sample from their copper polycrystal, and to Fred Fickett for supplying the copper crystal. Roy Bossingham oriented and cut the copper samples.

I would also like to thank the entire staff of TRIUMF for their efforts in delivering the beam to the experimenters and for the many other services which are necessary when performing work as visitors at their laboratory.

Finally, I would like to thank my family for encouraging my interest in science from an early age and for providing financial support during my undergraduate education.

This work was supported in part by the taxpayers of the United States through U.S. Department of Energy contracts DE-AC03-76SF0009 and AT03-81ER40004.

REFERENCES

1. J.H. Brewer, K.M. Crowe, F.N. Gygax and A. Schenck, in Muon Physics edited by Vernon W. Hughes and C.S. Wu, Vol. III, (Academic, New York, 1975).

2. J.H. Brewer and K.M. Crowe, Ann. Rev. Nucl. Part. Sci. 28 (1978) 239.

3. A. Schenck, in Nuclear and Particle Physics at Intermediate Energies edited by J.B. Warren, (Plenum, New York, 1976).

4. R.S. Hayano, Y.J. Uemura, J. Imazato, N. Nishida, T. Yamazaki and R. Kubo, Phys. Rev. B20 (1979) 850.

5. I.I. Gurevich, E.A. Mel'eshko, I.A. Muratova, B.A. Nikol'skii, V.S.Roganov, V.I. Selivanov and B.V. Sokolov, Phys. Lett. 40A (1972) 1 3.

6. V.G. Grebinnik, I.I. Gurevich, V.A. Zhukov, A.P. Manych, E.A. Mel'eshko, I.A. Muratova, B.A. Nikol'skii, V.I. Selivanov and V.A. Suetin, So.. Phys.-JETP 41 (1976) 777 [Zh. Eksp. Teor. Fiz. 68 (1975) 1548].

7. M. Camani, F.N. Gygax, W. Ruegg, A. Schenck and H. Schilling, Phys. Rev. Lett. 39 (1977) 836.

8. M. Camani, D.G. Fleming, F.N. Gygax, W. Ruegg, A. Schenck and H. Schilling, Hyperfine Int. 6 (1979) 265.

9. H. Schilling, Ph.D. Thesis, no. 5608, ETH Zurich (1980).

10. H. Schilling, M. Camani, F.N. Gygax, W. Ruegg, and A. Schenck, Hyperfine Int. 8 (1981) 675.

11. O. Hartmann, Phys. Rev. Lett. 39 (1977) 832.

12. A. Abragam, The Principles of Nuclear Magnetism, (Oxford, London, 1961), chapter X.

13. R. Kubo and K. Tomita, J. Phys. Soc. Japan 9 (1954) 888.

14. J.H. Van Vleck, Phys. Rev. 74 (1948) 1168.

15. O. Hartmann, E. Karlsson, K. Pernestal, M. Borghini, T.O. Niinikoski and L.O. Norlin, Phys. Lett. 61A (1977) 141.

16. H. Teichler, Phys. Lett. 64A (1977) 78.

17. H. Teichler, Phys. Lett. 67A (1978) 313.

18. H. Teichler, Hyperfine Int. 6 (1979) 251.

19. H. Teichler, in Exotic Atoms '79, Fundamental Interactions and Structure of Matter, edited by K. Crowe, J. Duclos, G. Fiorentini and G. Torelli (Plenum, New York, 1980), p. 283.

20. H. Teichler, Hyperfine Int. 8 (1981) 505.

21. C.P. Flynn and A.M. Stoneham, Phys. Rev. B1 (1970) 3966.

22. Yu. Kagan and M.I. Klinger, J. Phys. C7 (1974) 2791.

23. O. Hartmann, E. Karlsson, L.O. Norlin, T.O. Niinikoski, K.W. Kehr, D. Richter, J.-M. Welter, A. Yaouanc and J. Le Hericy, Phys. Rev. Lett. 44 (1980) 337.

24. O. Hartmann, Hyperfine Int. 8 (1981) 525.

25. O. Hartmann, L.O. Norlin, A. Yaouanc, J. Le Hericy, E. Karlsson and T.O. Niinikoski, Hyperfine Int. 8 (1981) 533.

26. C.W. Clawson, K.M. Crowe, S.E. Kohn, S.S. Rosenblum, C.Y. Huang, J.L. Smith and J.H. Brewer, Proceedings of LT-16, to be published in Physica (1982).

27. A.E. Pifer, T. Bowen and K.R. Kendall, Nucl. Instrum. Methods 135 (1976) 39.

28. C.J. Oram, J.B. Warren, G.M. Marshall and J. Doornbos, Nucl. Instrum. Methods 179 (1981) 95.

29. D.M. Garner, Ph.D. Thesis, Dept. of Chemistry, Univ. of British Columbia, 1979.

30. Available from the CERN program library, Division DD, CERN, CH 1211, Geneve 23, Switzerland.

31. T. Yamazaki, Hyperfine Int. 6 (1979) 115.

32. Y.J. Uemura, R.S. Hayano, J. Imazato, N. Nishida and T. Yamazaki, Solid State Comm. 31 (1979) 731.

33. We neglect the electron spins in the metal. They serve to create a small Knight shift of the muon precession frequency and a small Korringa relaxation.

34. J. Owen, M.E. Browne, W.D. Knight and C. Kittel, Phys. Rev. 102 (1956) 1501.

35. Abragam (op. cit., chapter IV) gives this in the form $\langle s_x(t)\rangle \propto \mathrm{tr}\, s_x s_x(t)$, from which our form for $\langle s_+(t)\rangle$ may be easily derived.

36. I.J. Lowe and R.E. Norberg, Phys. Rev. 107 (1957) 43.

37. A. Abragam, op. cit., chapter IV.

38. R. Kubo and T. Toyabe, in Magnetic Resonance and Relaxation, edited by R. Blinc, (North Holland, Amsterdam, 1967).

39. R.E. Walstedt and L.R. Walker, Phys. Rev. B9 (1974) 4857.

40. R. Kubo, Hyperfine Int. 8 (1981) 731.

41. T. McMullen and E. Zaremba, Phys. Rev. B18 (1978) 3026.

42. P.W. Anderson and P.R. Weiss, Rev. Mod. Phys. 25 (1953) 269.

43. Y.J. Uemura, M.S. Thesis, Department of Physics, University of Tokyo, 1979.

44. W.A. Zajc, private communication.

45. J.H. Brewer, private communication.

46. A.T. Fiory, Hyperfine Int. 8 (1981) 777.

47. F. Fickett, Mat. Sci. Eng. 14 (1974) 199.

48. H. Bruning and J. Le Hericy, to be published.

49. V.G. Grebinnik, I.I. Gurevich, A.I. Klimov, V.N. Majorov, A.P. Manych, E.V. Mel'nikov, B.A. Nikol'skii, A.V. Pirogov, A.N. Ponomarev, V.I. Selivanov, V.A. Suetin and V.A. Zhukov, Hyperfine Int. 6 (1979) 275.

50. O. Hartmann, E. Karlsson, L.O. Norlin, D. Richter, and T.O. Niinikoski, Hyperfine Int. 6 (1979) 289.

51. J.H. Brewer, E. Koster, A. Schenck, H. Schilling, and D.L. Williams, Hyperfine Int. 8 (1981) 671.

52. A.M. Stoneham, Hyperfine Int. 6 (1979) 211.

53. A.M. Stoneham, in Exotic Atoms '79, Fundamental Interactions and Structure of Matter, edited by K. Crowe, J. Duclos, G. Fiorentini and G. Torelli (Plenum, New York, 1980), p. 209.

54. D. Emin, Phys. Rev. Lett. 25 (1970) 1751.

55. D. Emin, Phys. Rev. B3 (1971) 1321.

56. David Emin, M.I. Baskes, and W.D. Wilson, Phys. Rev. Lett. 42 (1979) 791.

57. A. Yaouanc, Phys. Lett. 87A (1982) 423.

58. T. McMullen and B. Bergerson, Solid State Comm. 28 (1978) 31.

59. D. Richter, in Exotic Atoms '79, Fundamental Interactions and Structure of Matter, edited by K. Crowe, J. Duclos, G. Fiorentini and G. Torelli (Plenum, New York, 1980), p. 245.

60. S. Fujii and Y.J. Uemura, Solid State Comm. 26 (1978) 761.

61. S. Fujii, J. Phys. Soc. Japan 46 (1979) 1833.

62. V.G. Grebinnik, I.I. Gurevich, V.A. Zhukov, A.I. Klimov, V.N. Majorov, A.P. Manych, E. V. Mel'nikov, B.A. Nikol'skii, A.V. Pirogov, A.N. Ponomarev, V.I. Selivanov and V.A. Suetin, Pisma Zh. Eksp. Teor. Fiz. 25 (1977) 322.

63. E. Karlsson, Hyperfine Int. 8 (1981) 647.

64. H. Graf, G. Balzer, E. Recknagel, A. Weidinger and R.I. Grynszpan, Phys. Rev. Lett. 44 (1980) 1333.

65. K.W. Kehr, D. Richter, J.M. Welter, O. Hartmann, L.O. Norlin, E. Karlsson, T.O. Niinikoski, J. Chappert and A. Yaouanc, Hyperfine Int. 8 (1981) 681.

66. David Emin, Hyperfine Int. 8 (1981) 515.

67. K.G. Petzinger, R.L. Munjal, and E. Zaremba, Hyperfine Int. 6 (1979) 223.

68. K.W. Kehr, D. Richter, and G. Honig, Hyperfine Int. 6 (1979) 219.

69. T.O. Niinikoski, O. Hartmann, E. Karlsson, L.-O. Norlin, K. Pernestal, K.W. Kehr, D. Richter, E. Walker, and K. Schulze, Hyperfine Int. 6 (1979) 229.

70. K.G. Petzinger, Phys. Lett. 75A (1980) 225.

71. K.G. Petzinger, Hyperfine Int. 8 (1981) 639.

72. E. Karlsson, in Exotic Atoms '79, Fundamental Interactions and Structure of Matter, edited by K. Crowe, J. Duclos, G. Fiorentini and G. Torelli (Plenum, New York, 1980), p. 303.

73. O. Hartmann, E. Karlsson, L.O. Norlin, D. Richter and T.O. Niinikoski, Phys. Rev. Lett. 41 (1978) 1055.

74. P.W. Anderson, Phys. Rev. 109 (1958) 1492.

75. A. Browne and A.M. Stoneham, unpublished. (Preprint in μSR Newsletter 23 (1979) 1060.

Table I

Zero-field Hopping Rate
100-160 K

T(K)	$\nu(\mu s^{-1})$
100	0.022 ± 0.006
110	0.084 ± 0.016
120	0.125 ± 0.035
140	0.402 ± 0.023
160	0.699 ± 0.036

Table II

Transverse-field widths and asymmetries

Run	Sample	H(Oe)	T(K)	Hist.	A	$\sigma(\mu s^{-1})$
115	LBL	100	2.65±0.05	L	.2425(20)	.3144(58)
				R	.2543(20)	.3106(58)
				F	.2471(34)	.3002(101)
				B	.1966(16)	.3043(60)
121	LBL	100	4.2±0.1	L	.2451(15)	.3410(45)
				R	.2542(14)	.3359(43)
				F	.2552(26)	.3413(78)
				B	.1976(6)	.3388(45)
126	LBL	100	0.74±0.01	L	.2421(16)	.2786(46)
				R	.2545(16)	.2899(45)
				F	.2493(28)	.2833(81)
				B	.1935(13)	.2828(48)
128	CERN	100	4.2±0.02	L	.2414(16)	.3311(47)
				R	.2425(16)	.3441(51)
				F	.2513(27)	.3296(79)
				B	.1978(13)	.3394(49)
131	CERN	100	0.49±0.01	L	.2386(14)	.2439(40)
				R	.2406(15)	.2536(43)
				F	.2523(24)	.2544(67)
				B	.1936(12)	.2465(44)
135	CERN	100	1.1±0.05	L	.2403(16)	.2757(47)
				R	.2444(17)	.2824(49)
				F	.2552(27)	.2873(77)
				B	.1935(14)	.2914(53)
812	LBL	86	4.8±0.1	L	.2709(13)	.3280(34)
				R	.2689(11)	.3202(31)
				F	.2686(22)	.3270(70)
				B	.2104(14)	.3252(50)
815	LBL	40	4.8±0.1	L	.2669(22)	.3259(57)
				R	.2668(19)	.3198(51)
				F	.2713(38)	.3324(114)
				B	.2095(23)	.3437(84)
818	LBL	80	2.43±0.01	L	.2691(19)	.3032(52)
				R	.2676(17)	.3123(48)
				F	.2673(35)	.3166(108)
				B	.2118(21)	.3104(73)
819	LBL	80	0.61±0.01	L	.2656(17)	.2598(46)
				R	.2650(16)	.2617(42)
				F	.2648(31)	.2659(98)
				B	.2048(18)	.2567(65)

Table III

Zero-field Dipolar Width

Run	Sample	T(K)	Hist.	$\Delta_z(\mu s^{-1})$
114	LBL	0.46±0.002	F	.397(14)
			B	.390(10)
116	LBL	2.72±0.03	F	.392(10)
			B	.395(5)
117	LBL	0.50±0.007	F	.401(13)
			B	.397(12)
119	LBL	4.20±0.05	F	.361(11)
			B	.382(5)
125	LBL	0.73±0.01	F	.380(12)
			B	.389(8)
129	CERN	4.3±0.1	B	.359(5)
132	CERN	0.50±0.01	F	.381(11)
			B	.393(10)
134	CERN	1.10±0.01	F	.400(11)
			B	.389(8)
816	LBL	5.15±0.05	F	.397(7)
			B	.399(5)
817	LBL	2.35±0.03	F	.381(8)
			B	.385(5)
820 +822 +824	LBL	0.63±0.01	F	.399(7)
			B	.369(5)

Table IV

Zero-field Hopping Rates

Run	Sample	T(K)	Hist.	$\nu(\mu s^{-1})$	+error	-error	χ^2/NDF
114	LBL	0.46±0.002	F	.3349	70	214	179/144
			B	.2676	91	165	197/145
116	LBL	2.72±0.03	F	.1385	177	165	161/144
			B	.0990	96	96	169/145
117	LBL	0.50±0.007	F	.2942	396	361	178/144
			B	.3346	121	199	170/145
119	LBL	4.20±0.05	F	.2418	113	145	155/144
			B	.2031	175	138	147/145
125	LBL	0.73±0.01	F	.4417	390	230	130/144
			B	.5078	223	225	155/145
129	CERN	4.3±0.1	B	.1707	103	106	181/145
132	CERN	0.50±0.01	F	.4070	169	299	137/144
			B	.4135	171	168	157/145
134	CERN	1.10±0.01	F	.3594	206	214	125/144
			B	.3610	143	137	152/145
816	LBL	5.15±0.05	F	0.0000	31	-	185/141
			B	.0595	-	290	181/141
817	LBL	2.35±0.03	F	.2264	-	106	193/141
			B	.2675	138	109	145/141
820 +822 +824	LBL	0.63±0.01	F	.3577	129	170	229/141
			B	.4873	186	139	149/141

Table V

Zero- and Transverse-field Hopping Rates

T(K)	$\nu_{zf}(\mu s^{-1})$	$\nu_{t}(\mu s^{-1})$
4.8 ± 0.1		0.409 ± 0.031
5.14 ± 0.05	0.092 ± 0.012	
2.43 ± 0.01		0.509 ± 0.015
2.35 ± 0.03	0.261 ± 0.014	
0.61 ± 0.01		0.822 ± 0.042
0.63 ± 0.01	0.489 ± 0.034	

Figure captions

(1) Transverse-field relaxation rate vs. temperature in polycrystalline copper. The rate $\Lambda(T)$ is defined in a shape-independent manner as the inverse of the time taken for the polarization to decay to 1/e of its initial value. a) Λ vs. T. b) Arrhenius plot of correlation times obtained from 1/e times of Eq. III.11. (From Ref. 5.)

(2) Potential energy for hydrogenic interstitials in a rigid Cu lattice. The ground state energies of the proton and the μ^+ at the octahedral (O) site are indicated. The well at the tetrahedral (T) site is too shallow for a μ^+ bound state to exist. (From Ref. 19.)

(3) Range curve for surface μ^+ in mylar. This represents the fraction of the μ^+ beam surviving after traversing a given amount of material. (From Ref. 2.)

(4) Plan view of the "Eagle" μ^+SR spectrometer vacuum chamber with cryostat.

(5) Data acquisition electronics. Not shown are scaler connections and delay cables necessary for pulse timing.

(6) Timing diagrams for typical events. T represents the adjustable data gate length.

(7) Schematic view of ^{3}He refrigerator installed in the tail of the ^{4}He gas-flow cryostat. Not shown is the 77 K radiation shield with a 0.0003" aluminized Mylar window.

(8) a) Example of a "raw" transverse-field μ^+SR spectrum, taken in copper at 83 Oe and 4.2 K. b) The same data reduced to show the asymmetry.

(9) a) Zero-field and b) transverse-field relaxation functions with $\Delta_z^2 = 5/2\Delta_x^2$. In both cases the time axis is $\Delta_z t$. The curves in a) are from the theory of Ref. 4, and those in b) are from Eq. III.11.

(10) Static transverse dipolar width vs. magnetic field. (From Ref. 7.)

(11) Arrhenius plot of hopping rate in copper derived from zero-field relaxation near 100 K.

(12) Transverse-field line width in copper at low temperature. Our data are superimposed on that of Hartmann, et. al. (Ref. 23). For our data, the errors are smaller than the point sizes.

Ref. 23 -- Open squares: Cu polycrystal, 520 Oe
Open circles: Al polycrystal, 120 Oe
Filled circles: Al polycrystal, 520 Oe

This work -- Filled triangles: Cu crystal, 80 Oe
Open triangles: Cu polycrystal, 80 Oe
Crossed circle: Al Polycrystal, 80 Oe

(13) Zero-field width vs. temperature, from weighted averages of forward and backward spectra. Filled points are LBL copper crystal, open points are CERN copper used in Ref. 23.

(14) Hopping rate from zero-field relaxation at low temperature. Filled points are from the LBL copper, and open points are from the CERN copper used in Ref. 23.

(15) Backward asymmetry in zero field at several temperatures.

(16) Zero-field and transverse-field hopping rates in copper, from simultaneous fits to forward and backward spectra.

(17) Schematic plot of transverse-field width vs. temperature for trap-limited diffusion. The dotted line indicates the effect of increasing the trap concentration, thereby reducing T_t.

(18) Zero-field relaxation functions for trap-limited diffusion. (From Ref. 71.)

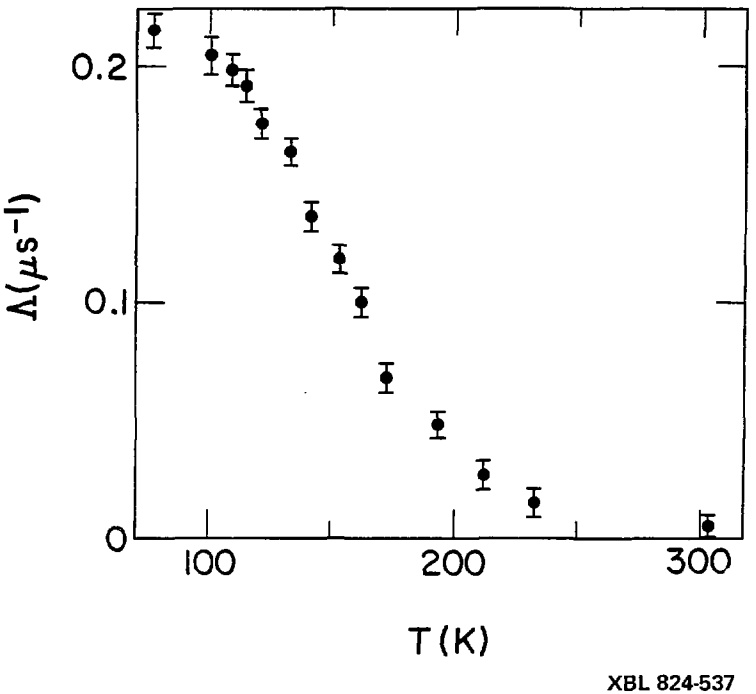

Fig. 1a

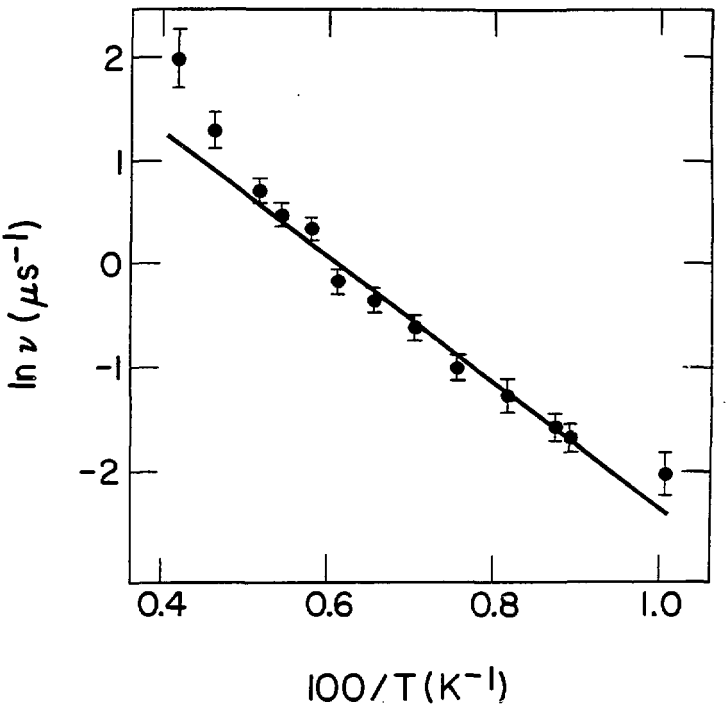

Fig. 1b

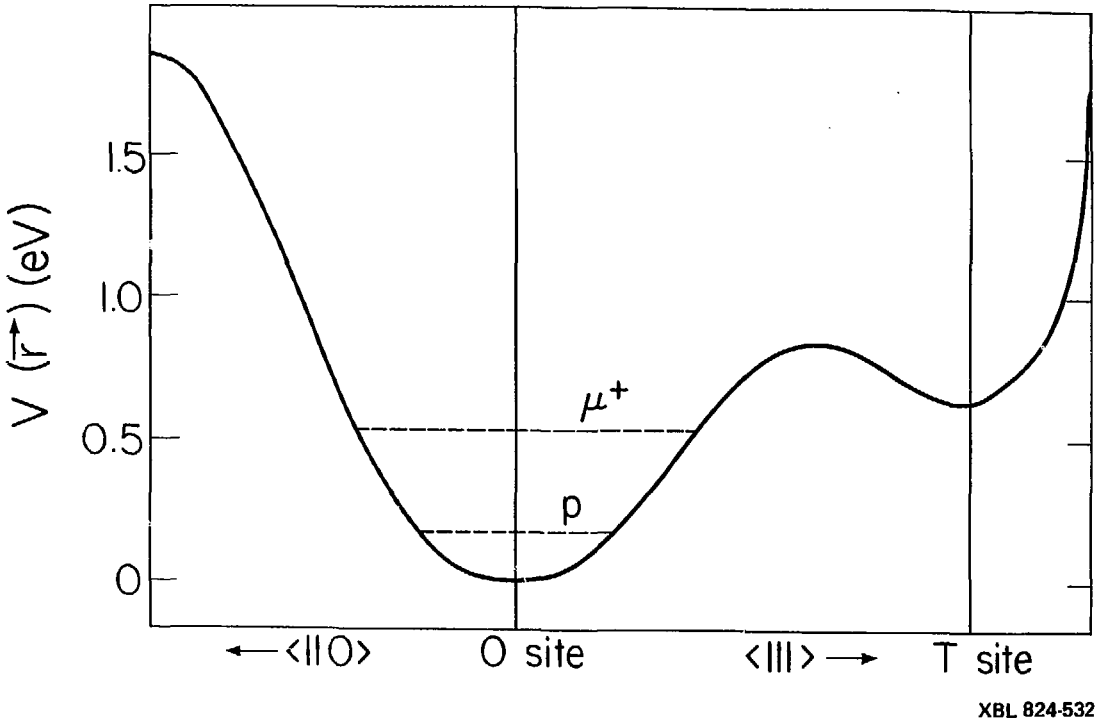

Fig. 2

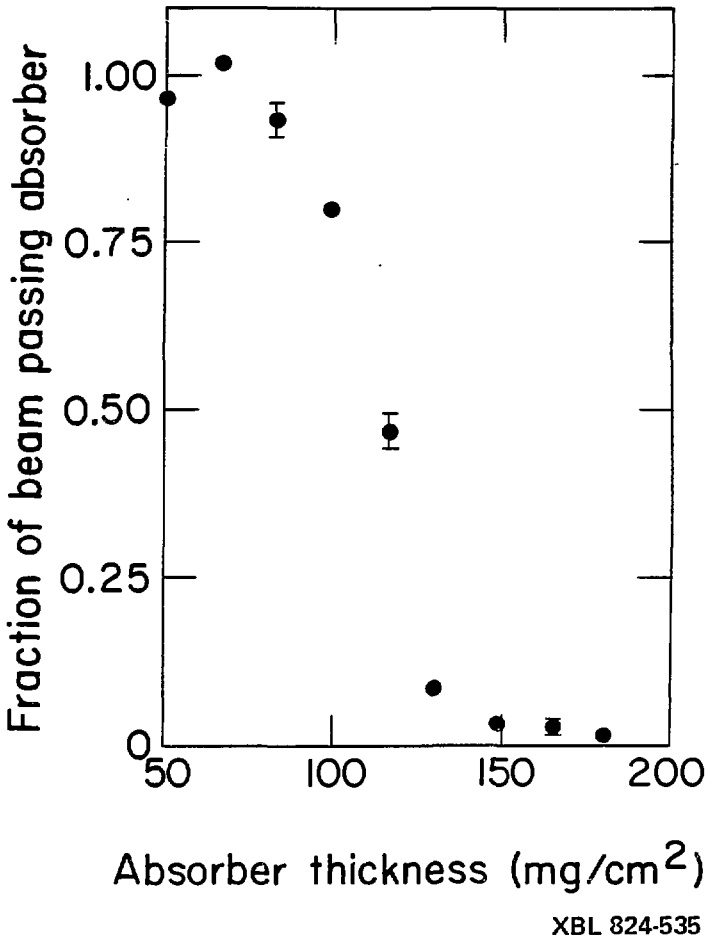

XBL 824-535

Fig. 3

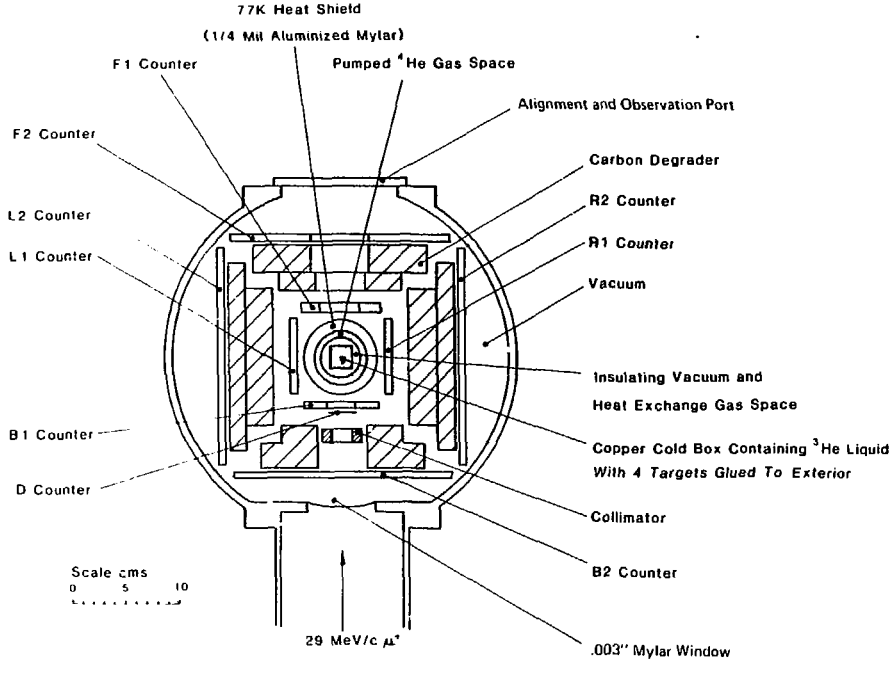

XBL 817-10875

Fig. 4

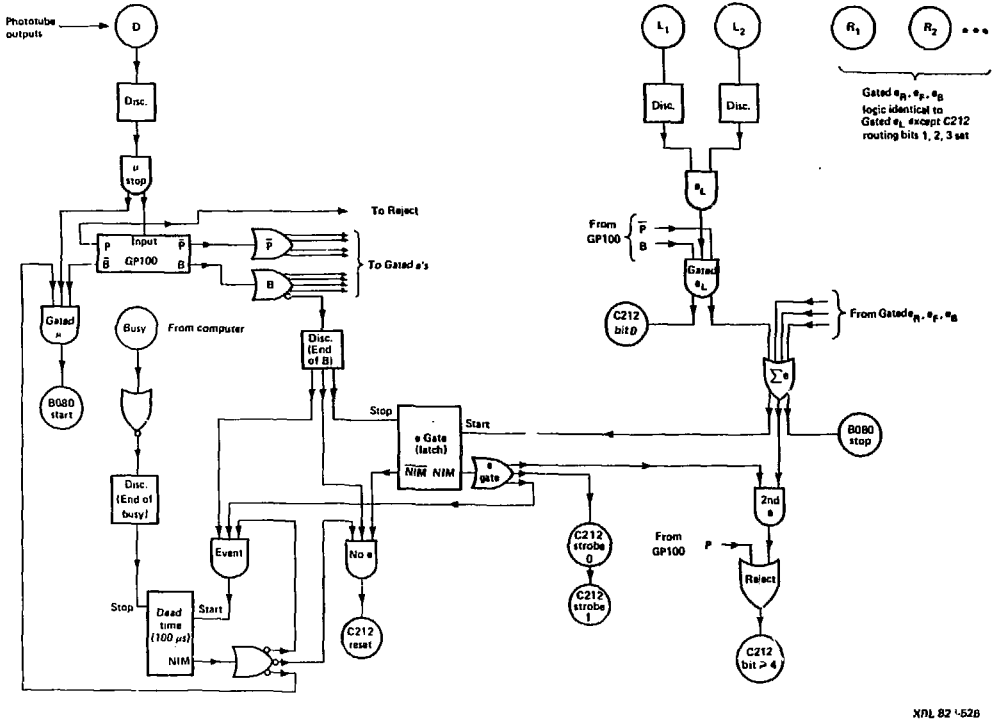
Phototube outputs
D
Disc.
μ stop
To Reject
Input GP100
To Gated e's
Gated μ
Busy
From computer
B080 start
Disc. (End of Bi
Disc. (End of busy)
Stop
e Gate (latch)
Start
NIM NIM
e gate
Event
No e
Dead time (100 μs)
NIM
C212 reset
C212 strobe 0
C212 strobe 1
From GP100
2nd e
Reject
C212 bit > 4
L1
L2
Disc.
Disc.
eL
From GP100
Gated eL
C212 bit 0
From Gate eR . eF . eB
Σe
B080 stop
R1
R2
Gated eR . eF . eB
logic identical to Gated eL except C212 routing bits 1, 2, 3 set
XBL 82 1528

Fig. 5

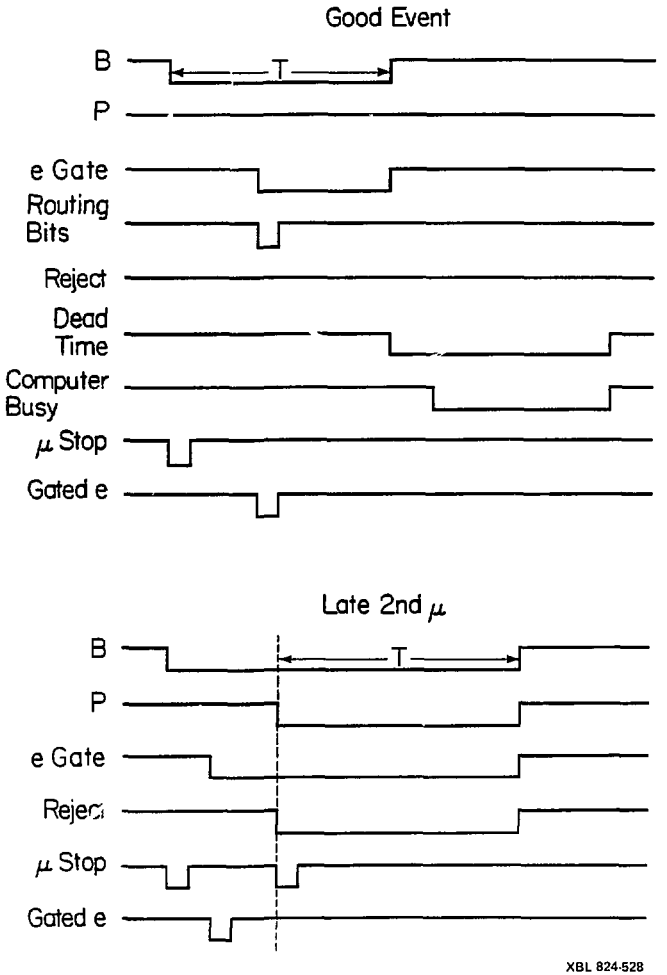

Fig. 6
(continued)

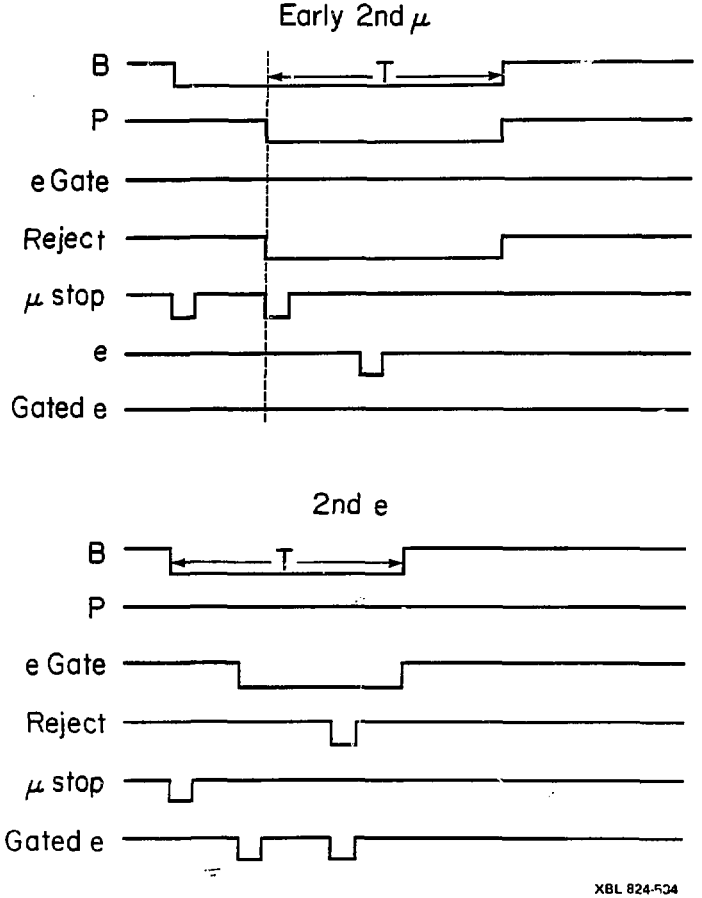
Early 2nd μ
B
T
P
e Gate
Reject
μ stop
e
Gated e
2nd e
B
T
P
e Gate
Reject
μ stop
Gated e
XBL 824-534

Fig. 6

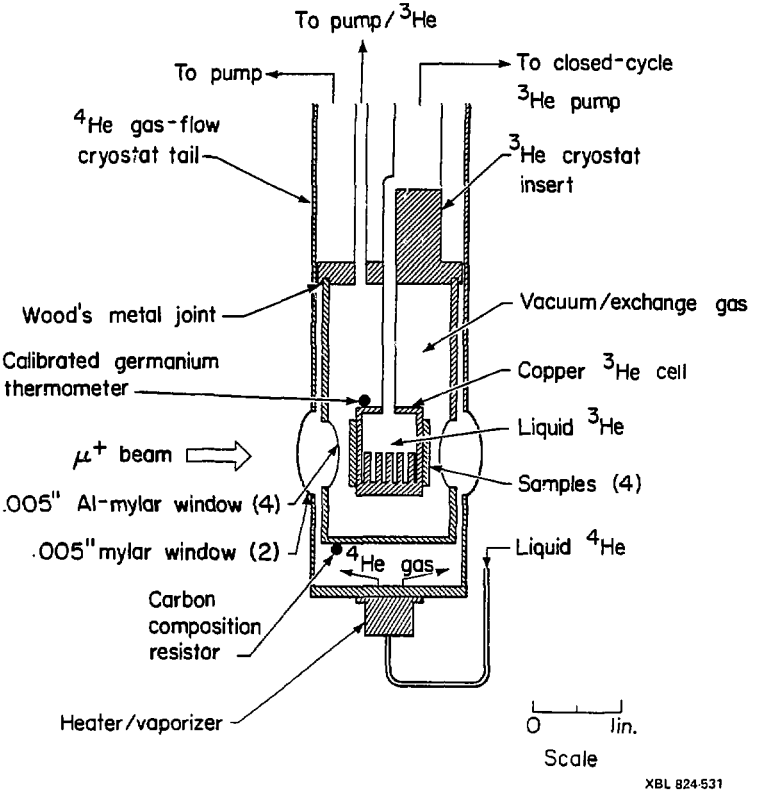
To pump/^{3}He
To pump
To closed-cycle
^{3}He pump
^{4}He gas-flow
cryostat tail
^{3}He cryostat
insert
Wood's metal joint
Vacuum/exchange gas
Calibrated germanium
thermometer
Copper ^{3}He cell
Liquid ^{3}He
μ^+ beam
Samples (4)
.005" Al-mylar window (4)
.005" mylar window (2)
Liquid ^{4}He
^{4}He gas
Carbon
composition
resistor
Heater/vaporizer
0
1in.
Scale
XBL 824-531

Fig. 7

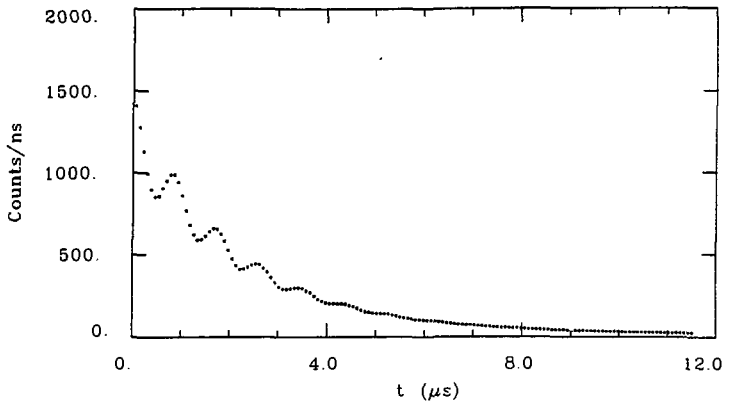
2000.
1500.
1000.
500.
0.
Counts/ns
0.
4.0
8.0
12.0
t (μs)

(a)

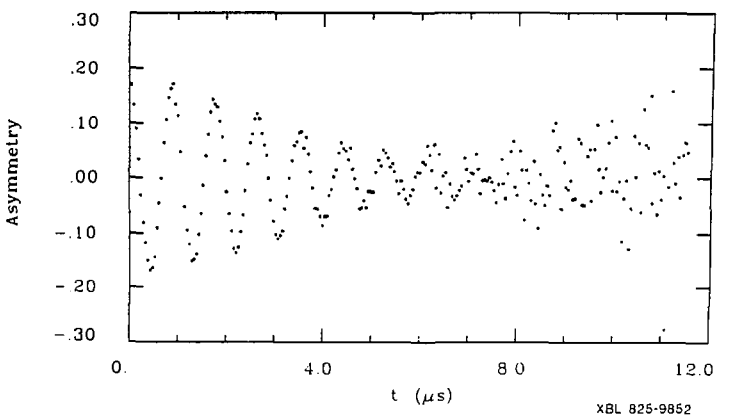
.30
.20
.10
.00
-.10
-.20
-.30
Asymmetry
0.
4.0
8.0
12.0
t (μs)
XBL 825-9852

(b)

Fig. 8

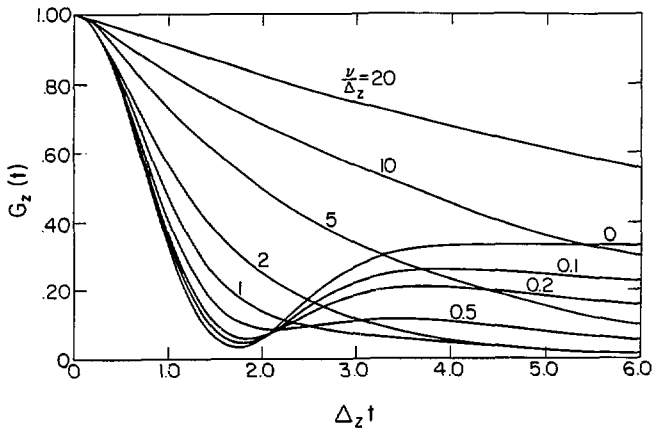
1.00
.80
.60
.40
.20
0
$G_z(t)$
$\frac{\nu}{\Delta_z}$=20
10
5
2
1
0.5
0.2
0.1
0
0
1.0
2.0
3.0
4.0
5.0
6.0
$\Delta_z t$

(a)

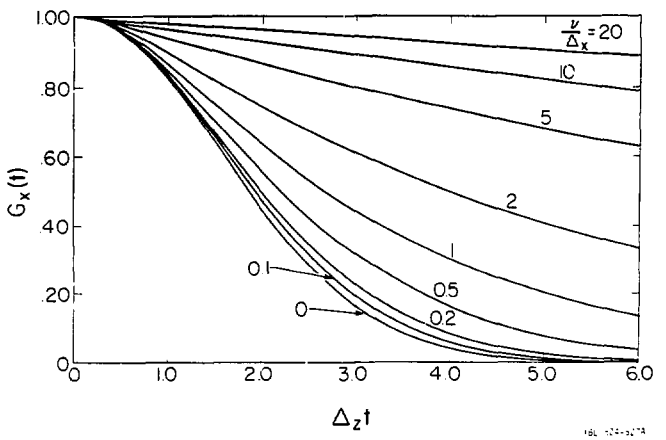
1.00
.80
.60
.40
.20
0
$G_x(t)$
$\frac{\nu}{\Delta_x}$=20
10
5
2
1
0.5
0.2
0.1
0
0
1.0
2.0
3.0
4.0
5.0
6.0
$\Delta_z t$

(b)

Fig. 9

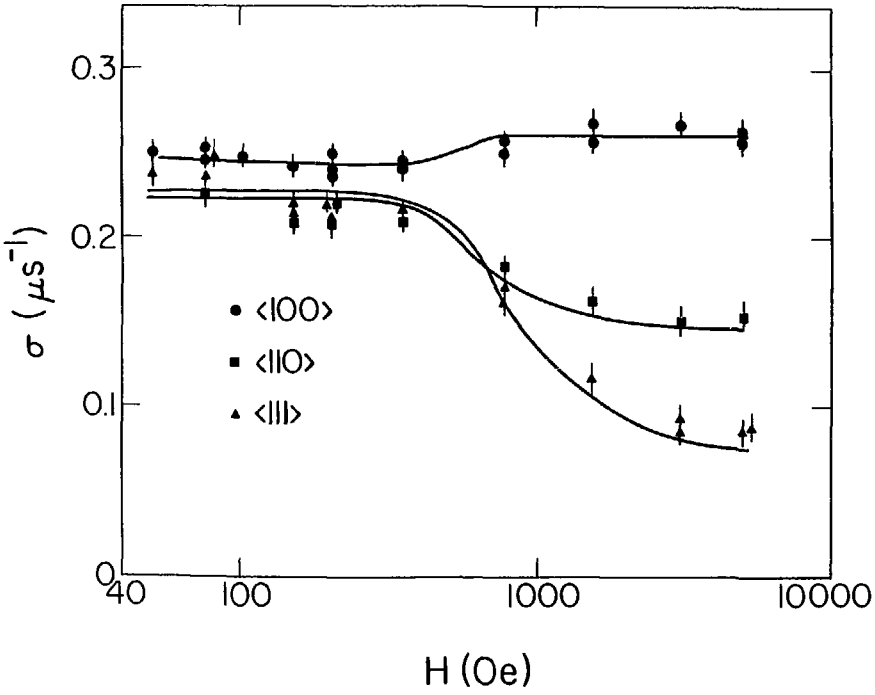

XBL 824-533

Fig. 10

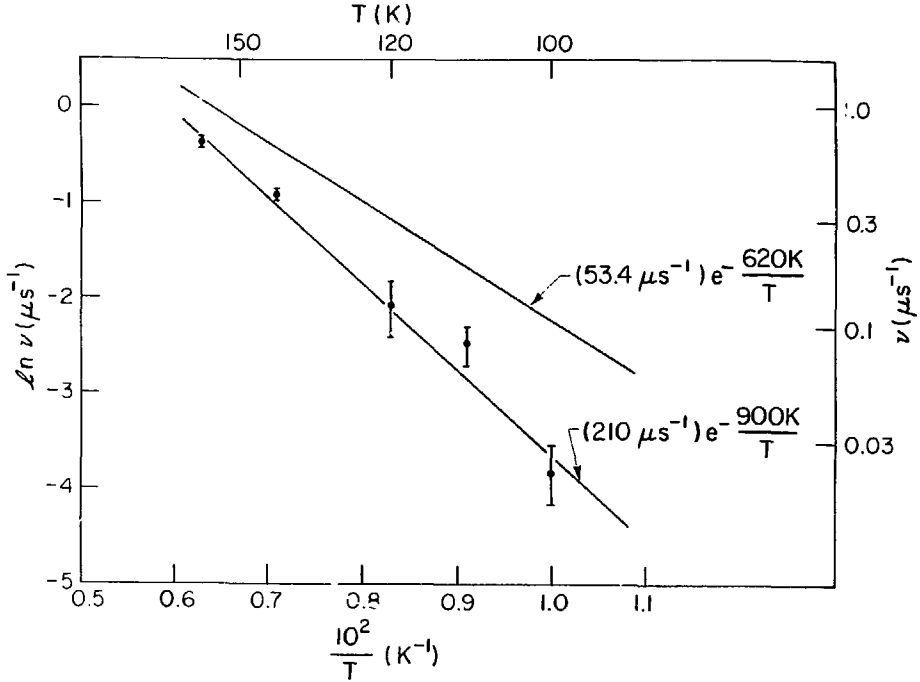

XBL 825-557

Fig. 11

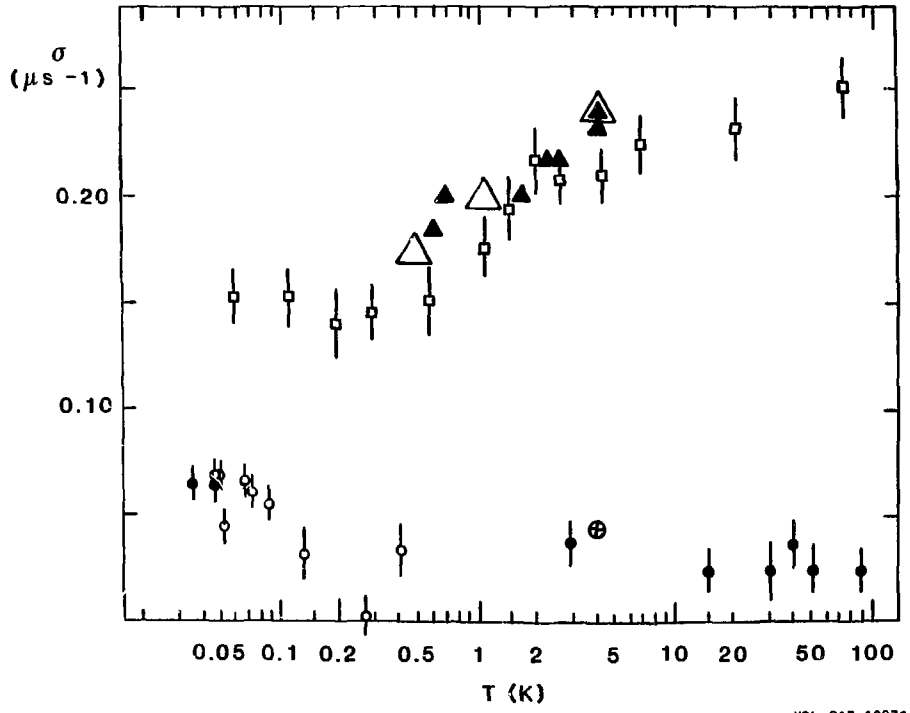

Fig. 12

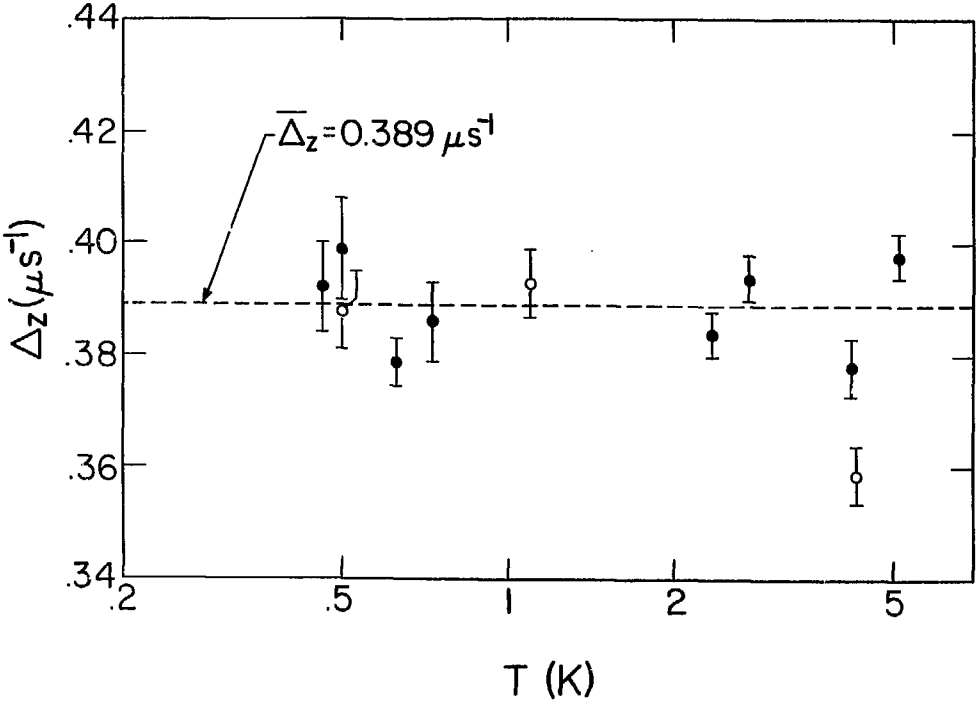
.44
.42
.40
.38
.36
.34
.2
.5
1
2
5
$\overline{\Delta}_z = 0.389\ \mu s^{-1}$
$\Delta_z(\mu s^{-1})$
T (K)
XBL 824-529

Fig. 13

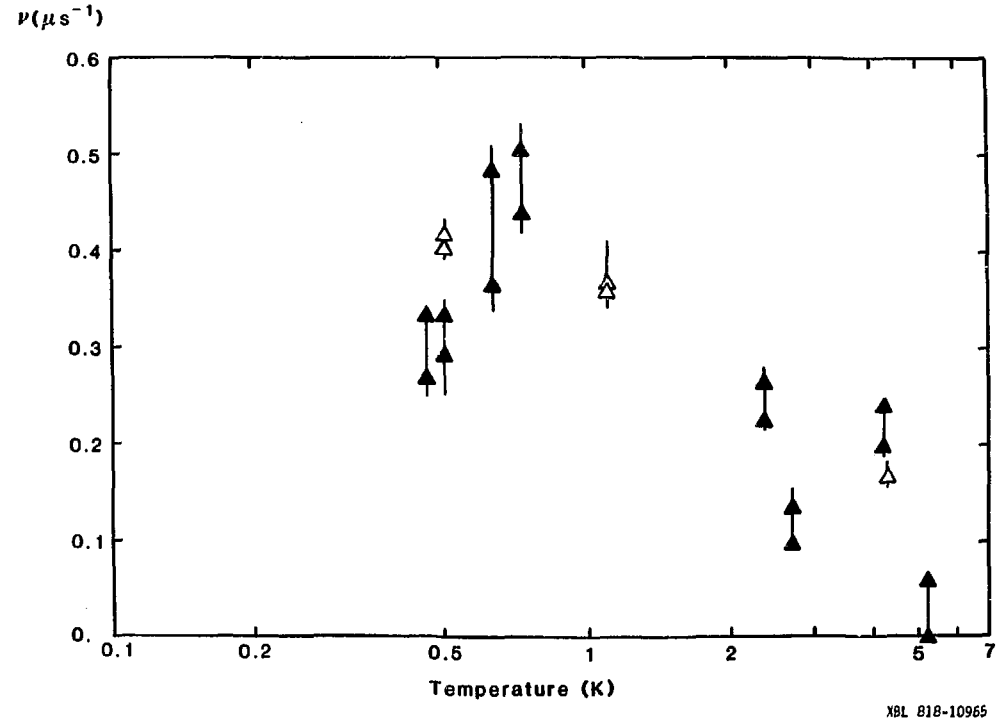
$\nu(\mu s^{-1})$
0.6
0.5
0.4
0.3
0.2
0.1
0.
0.1
0.2
0.5
1
2
5
7
Temperature (K)
XBL 818-10965

Fig. 14

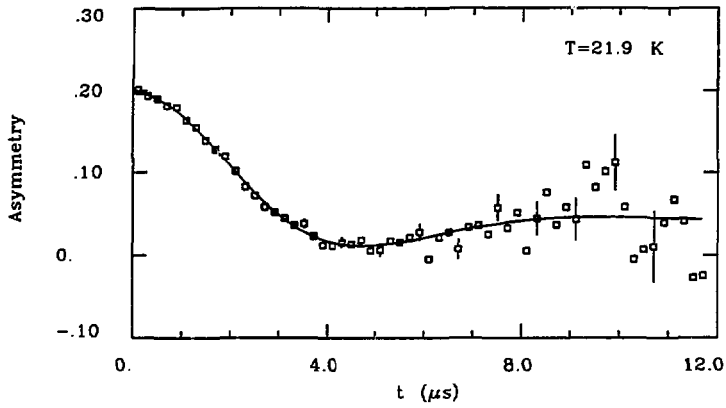

(a)

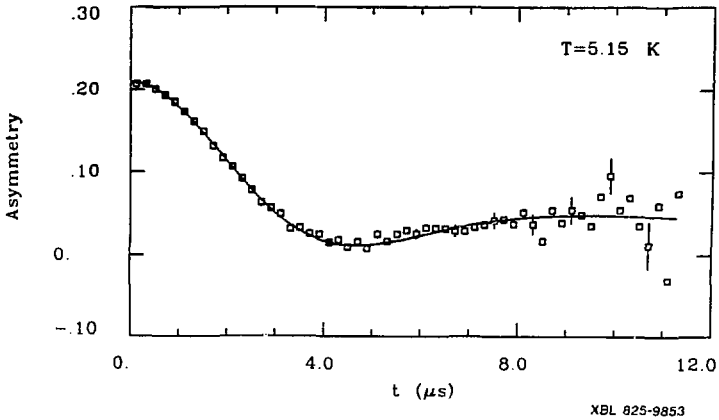

(b)

Fig. 15
(continued)

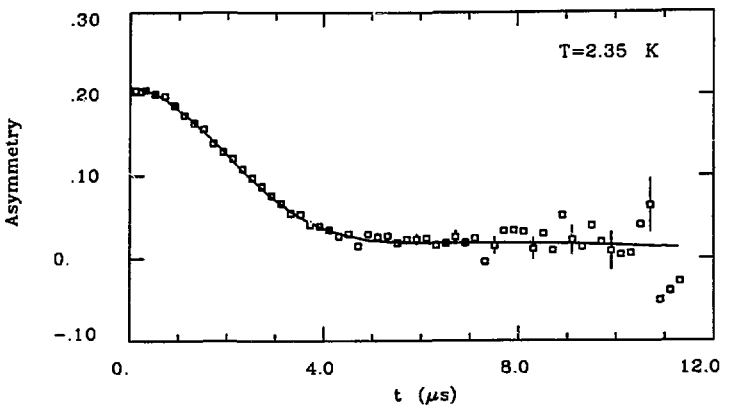
.30
.20
.10
0.
-.10
Asymmetry
T=2.35 K
0.
4.0
8.0
12.0
t (μs)

(c)

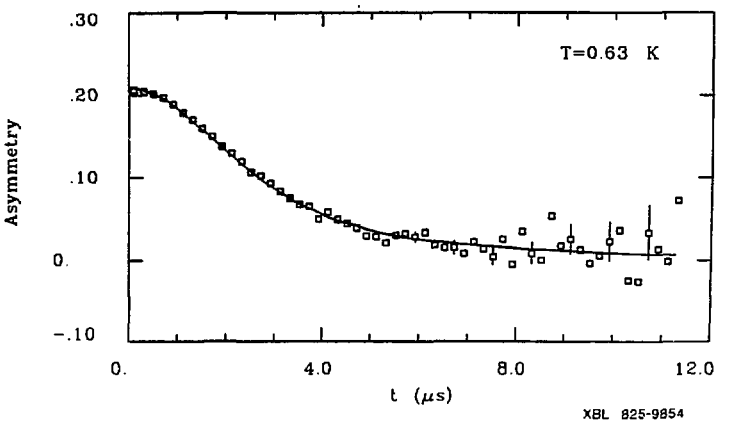
.30
.20
.10
0.
-.10
Asymmetry
T=0.63 K
0.
4.0
8.0
12.0
t (μs)
XBL 825-9854

(d)

Fig. 15

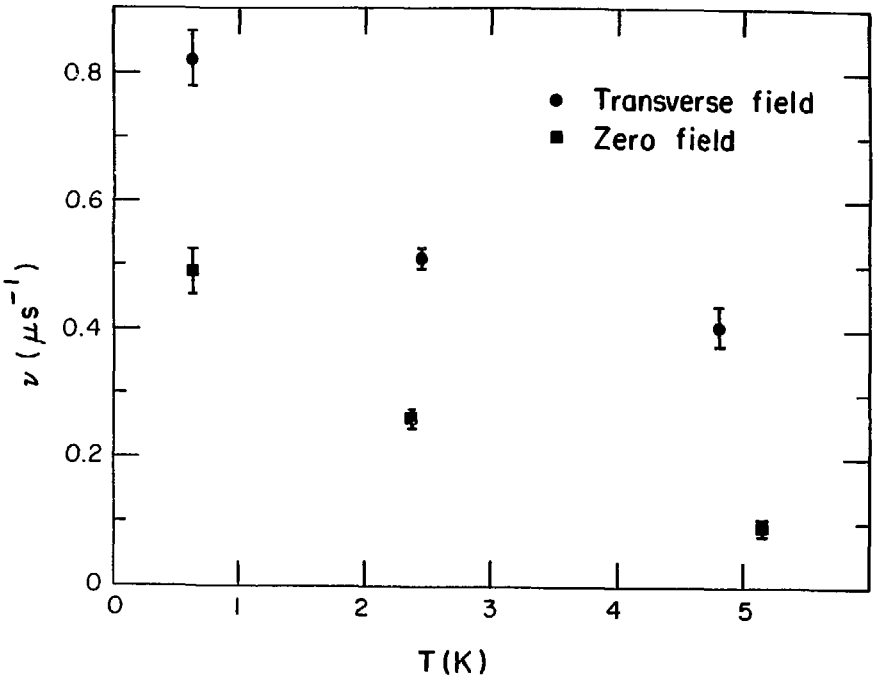

XBL 825-559

Fig. 16

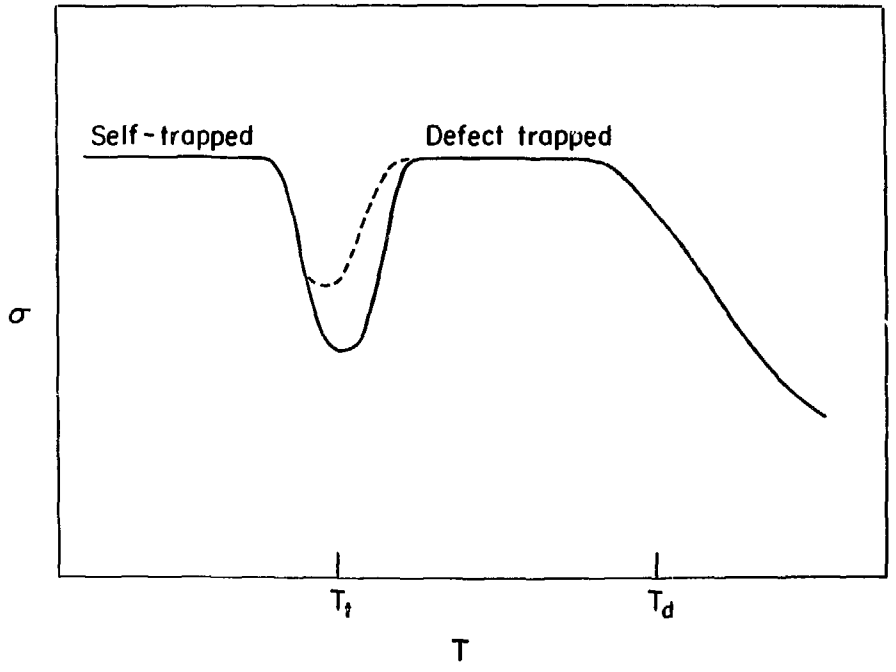

XBL 825-556

Fig. 17

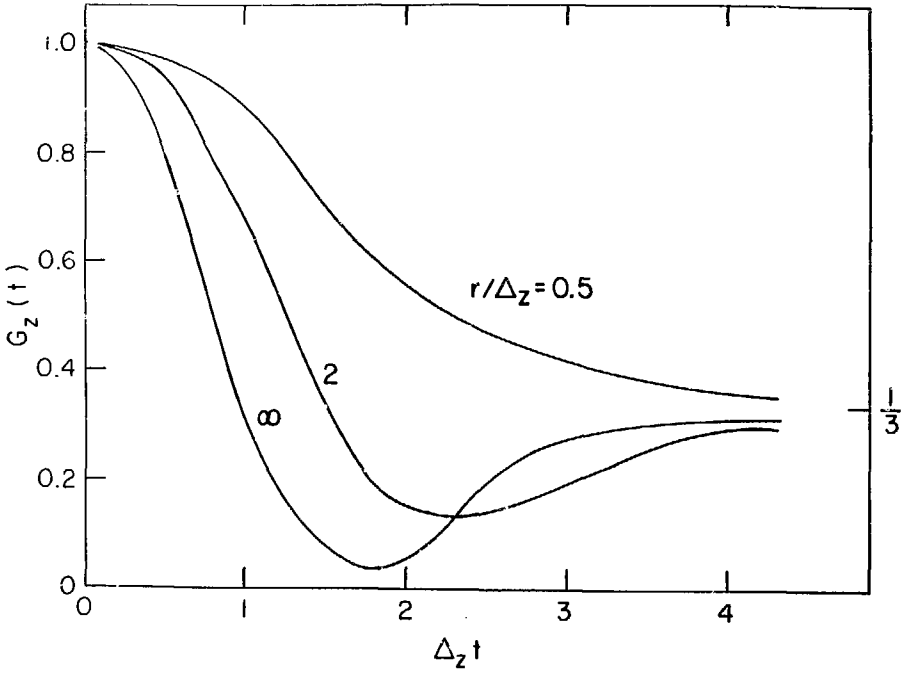

XBL 825-558

Fig. 18

TECHNICAL INFORMATION DEPARTMENT
LAWRENCE BERKELEY LABORATORY
UNIVERSITY OF CALIFORNIA
BERKELEY, CALIFORNIA 94720